

# Synthetic construction of the Hopf fibration in the double orthogonal projection of the 4-space

Michal Zamboj

Charles University, Faculty of Education, Department of Mathematics  
and Mathematical Education

M. D. Rettigová 4, 116 39 Prague 1, Czech Republic  
michal.zamboj@pedf.cuni.cz

January 12, 2021

## Abstract

A mapping between circles on a 3-sphere and points on a 2-sphere is well known by topologists as the Hopf fibration. While the 2-sphere is embedded in a 3-space, to visualize the 3-sphere, the 4-dimensional Euclidean space is needed. Visualizations using computer graphics based on their analytic representations became popular in the last decades. Instead, for purely synthetic constructions, we apply the recently introduced method of visualization of the 4-space by its double orthogonal projection onto two mutually perpendicular 3-spaces to investigate the Hopf fibration as a four-dimensional relation without analogy in lower dimensions. In this paper, the double orthogonal projection method is used for direct synthetic construction of the fibers of a 3-sphere from the corresponding points on a 2-sphere. The fibers of great circles on the 2-sphere create nested tori visualized in a stereographic projection into the modeling 3-space. The step-by-step construction is supplemented by dynamic 3D models showing simultaneously the 3-sphere, 2-sphere, and stereographic images of the fibers and mutual interrelations. Each step of the synthetic construction is supported by its analytic representation to highlight connections between both interpretations.

**Keywords:** Hopf fibration; Hopf tori; four-dimensional visualization; stereographic projection; synthetic construction

# 1 Introduction

Mathematical visualization is an important brick in the wall of understanding mathematical concepts. While analytic representations are convenient for proofs and analyses of properties, synthetic visualizations are essential for intuitive exploration and hypothesis making. Four-dimensional mathematical objects, as a whole as they may be, are beyond our three-dimensional imagination. However, this is not an obstacle for mathematical description and studying such abstract objects. Furthermore, using modeling tools of computer graphics, we are able to construct image representations of four-dimensional objects to enhance their broader understanding. While many multi-dimensional mathematical objects are natural generalizations of less-dimensional cases, the object of our study — the Hopf fibration, is beyond this border. The Hopf fibration was introduced

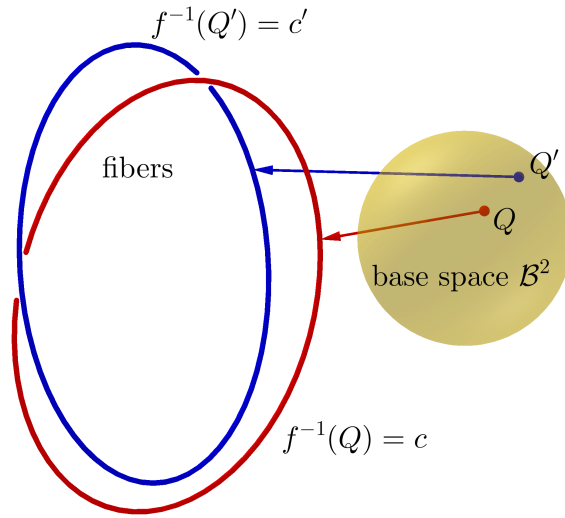


Fig. 1: Illustration of the Hopf fibration. Two distinct points  $Q$  and  $Q'$  on the 2-sphere  $\mathcal{B}^2$  correspond to circular fibers  $c$  and  $c'$ .

by Hopf (1931, 1935) and defines a mapping between spheres of different dimensions. In this paper, we restrict ourselves to a correspondence between spheres embedded in four and three-dimensional spaces. To each point on a 2-sphere in a three-dimensional space is assigned a circular fiber on a 3-sphere in the four-dimensional space. The standard method to visualize the fibers on the 3-sphere is to project them into a three-dimensional space via stereographic projection, in which we can also grasp the topological nature of the Hopf fibration. Two distinct points on a 2-sphere correspond to disjoint circular fibers on the 3-sphere and their stereographic images are linked circles (Fig. 1). Considering points along a circle on the 2-sphere, their corresponding circles on the 3-sphere form a torus (Fig. 2).

The second face of our interpretation is the method of visualization itself. Instead of

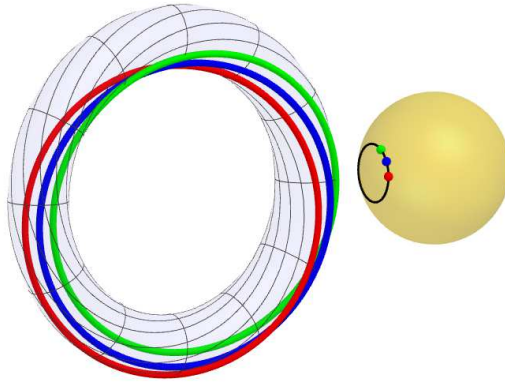


Fig. 2: The stereographic images of circular fibers corresponding to points on a circle on the base 2-sphere  $\mathcal{B}^2$  are linked Villarceau circles on a torus.

visualizing an analytic representation of a studied object, we create the object constructively point-by-point directly in a graphical environment. To do so, we use generalized techniques of classical descriptive geometry to create three-dimensional images of four-dimensional objects. Our constructions or models are technically impossible to create with hands without computer graphics. For this purpose, we use interactive (or dynamic) 3D geometry software in which the images are placed in a virtual three-dimensional modeling space, and the observer is able to reach any point of this space and rotate views. This may be achieved by manipulation of the viewpoint in the graphical interface. Furthermore, in the presented models, the user can interactively manipulate (or animate) some parts or parameters of the model and observe the instant changes of the dependant objects.<sup>1</sup>

Therefore, we believe in the existence of two (not necessarily disjoint) groups that could benefit from our paper: members of computer society, for whom we present the method of constructive visualization applied to the example of the Hopf fibration; mathematicians, or students of mathematics, for whom we give the synthetic construction and interactive graphical models for better understanding and further intuitive exploration of the Hopf fibration.

## 1.1 Related work

Due to the use of a 3-sphere, embedded in  $\mathbb{R}^4$  or  $\mathbb{C}^2$ , the construction of the Hopf fibration

---

<sup>1</sup>Further on, by interactive models or visualizations, we mean models with dynamically manipulable elements. Not to be confused with time-varying interactivity, which is often used in four-dimensional visualization.

is usually performed in an abstract algebraic language. However, recent research in computational geometry and graphics based on analytic representations brought partial video animations of the mapping or models of stereographic images and visualizations in various software. Koçak and Laidlaw (1987) described stereographic images of the Hopf fibration on the front covers of *Mathematical Intelligencer*, vol. 8, no. 3 and vol. 9, no. 1, taken from their pioneering computer-generated film projects with Banchoff, Bisshopp, and Margolis. Banchoff (1990) wrote an illustrated comprehensive book on the fourth dimension, and its front cover is, again, an inspiring picture of the Hopf fibration from his film. Moreover, emphasizing the computer visualization of the Hopf fibration, Banchoff (1988) constructed stereographic images of Pinkall's tori of given conformal type. The primary inspiration for writing this paper was another film — Dimensions by Alvarez et al. (2008) in which the Hopf fibration is well explained and visualized in separate models. Coincidentally, another front cover — of the *Notices of the AMS*, vol. 44, no. 5; was inspired by explanatory illustrations created in *Wolfram Mathematica* published by Kreminski (1997) in the context of the structure of the projective extension of the real 3-space  $\mathbb{RP}^3$ . Popular visualization of the Hopf fibration showing points on the base 2-sphere and corresponding stereographic images of the fibers was created by Johnson (2011) in Sage. Johnson's code was modified by Chinyere (2012) to visualize similar fibration with trefoil knots as fibers instead of circles.

The visual aspect is strongly accented by Hanson (2006) (pp. 80-85 and 386-392) to visualize quaternions on a 3-sphere, and the author also describes them using Hopf fibrations. Visualizations of the Hopf fibrations are used with favor in applications in topology in relation to the Heegaard splitting of a 3-sphere by Canlubo (2017), with the use of quaternions in physics by O'Sullivan (2015), and to describe motion in robotics by Yershova et al. (2010). Black (2010) in chapter 6 of his dissertation, showed, based on analytic representation, similar orthogonal projections of tori as do we, and supplemented them with animations.

Interactive tools used for visualization of 2-dimensional images of four-dimensional objects from different viewpoints in the 4-space are developed and applied by Zhou (1991). Heng (1992) wrote another early-stage complex thesis (supervised by Hanson) on the use of interactive mathematical visualization techniques in computer graphics applied to the exploration of 3-manifolds. The continuous development of interactive frameworks and methods of four-dimensional visualization is also apparent in further works co-authored by Hanson (e.g., in Hanson et al. (1999); Zhang and Hanson (2007), and with visualizations of a flat torus embedded in 4D from different viewpoints in Thakur and Hanson (2007); Chu et al. (2009)).

In this exposition, we use the language and elementary constructions in the double orthogonal projection described in Zamboj (2018a), and the constructions of sections of four-dimensional polytopes, cones, and spheres published in the consecutive articles

## 1.2 Contribution

In a broader sense, we present an application of a method of visualization and computer graphics as a vital perspective for constructing and examining a phenomenon described in the 4-space with no analogy in lower dimensions. In this paper, the method of double orthogonal projection is used to create a purely synthetic graphical construction of the Hopf fibration. The paper contributes to the field in two directions: a novel graphical construction of the Hopf fibration and the application of the double orthogonal projection. In contrast to previous works on visualization of the Hopf fibration, in which separate illustrations created from analytic representations were graphical results or explanatory additions, we use mathematical visualization via the double orthogonal projection as a tool to synthetically construct the fibration. For this purpose, we revisit the existential analytical definition of the Hopf fibration (points on a circle on a 3-sphere map to a point on a 2-sphere, given by expression (5)), which gives us the solved puzzle, and we decompose it into pieces to add the missing synthetic aspect. Afterward, we propose an elementary step-by-step construction of the inverse process. From points on the 2-sphere, we construct fibers of the 3-sphere with the use of only elementary (constructive) geometric tools. On top of that, we construct the resulting stereographic images of the fibers in one complex graphical interpretation. Even though stereographic images are common for visualization of the Hopf fibration, we construct them synthetically and use them to confirm our results and observations. At last, the method of visualization is applied to provide a graphical analysis of the properties of cyclic surfaces on a 3-sphere. Our constructions (Figs. 8–12, 14–17) are supplemented by interactive 3D models in *GeoGebra 5* (see online GeoGebra Book Zamboj (2019c)).<sup>2</sup> The final visualizations (Figs. 18 and 20) and videos (Suppl. Files 8 and 9) are created in *Wolfram Mathematica* for better graphical outcome. Throughout the paper, our synthetic visual approach is supported by the given analytical background to enrich the overall understanding of the Hopf fibration.

## 1.3 Paper Organization

The paper is organized as follows: The analytic definition and properties of the Hopf fibration are introduced in Section 2. In Section 3, we briefly describe images of a 3-sphere in the double orthogonal projection and construct its stereographic image. In the main part, Section 4, the synthetic construction of a Hopf fiber on a 3-sphere, corresponding to a point on a 2-sphere is given with only the use of elementary tools. The resulting double

---

<sup>2</sup>The software *GeoGebra 5* is used due to its general accessibility, but any other 3D interactive (dynamic) geometry software may be used for the same outcomes. For the overall understanding, we strongly recommend following the 3D models simultaneously with the text.

orthogonal projection and stereographic images of tori on the 3-sphere corresponding to two families of circles on the 2-sphere are described in Section 5. After the conclusion with perspectives on future work, we attach Appendix with parametrization relevant to figures.

## 2 Mathematical background

Fibrations are studied in algebraic topology. They consist of the total space, base space, fiber, and a projection from the total space onto the base space. Let us consecutively define the necessary terms on the following lines.

Let us have a collection of sets  $X_i$  for each index  $i$  in an index set  $I$ . The set of functions  $f : I \rightarrow \bigcup_{i=1} X_i$  such that  $f(i) \in X_i$ , for each  $i \in I$  is called the *Cartesian* (or *direct*) *product* of the family of sets  $\{X_i\}_{i \in I}$ . The Cartesian product is denoted by  $\prod_{i \in I} X_i$  or  $X_1 \times X_2 \times \dots$ .

A *topological space* is an ordered pair  $(X, \tau)$ , where  $X$  is a set and  $\tau$  is a collection of subsets of  $X$  satisfying the following conditions:

1. The empty set and  $X$  belong to  $\tau$ .
2. Arbitrary unions of elements in  $\tau$  belongs to  $\tau$ .
3. The intersection of any finite number of sets in  $\tau$  belongs to  $\tau$ .

$\tau$  is called the *topology* on  $X$  of the topological space  $(X, \tau)$ .

Let us have topological spaces  $\mathcal{T}$  and  $\mathcal{B}$  and a continuous surjective mapping  $f : \mathcal{T} \rightarrow \mathcal{B}$ . The ordered triple  $(\mathcal{T}, f, \mathcal{B})$  is called the *fiber space* or *fibration*,  $\mathcal{T}$  is the *total space*,  $\mathcal{B}$  is the *base space* and  $f$  is the *projection* (or *fibration*<sup>3</sup>) *of the fibre space*. The inverse image of a point (element) of the base space  $\mathcal{B}$  in the projection  $f$  is the *fiber above this point*.

A *3-sphere* is the three-dimensional boundary of a 4-ball in the four-dimensional Euclidean space. It is a natural generalization of a 2-sphere as the two-dimensional surface around a ball in the three-dimensional Euclidean space.

---

<sup>3</sup>Note that the term fibration is sometimes used as the whole triple, and sometimes as the mapping. With respect to the Hopf fibration, we freely use both, since it should not cause any confusion throughout the paper.

Let us describe some elementary examples of fibrations. Hanson (2006), p. 386, illustrated a trivial fibration as a shag rug, where the backing of the rug is the base space, and the threads are fibers. Similarly, a spiky massage ball has the 2-sphere as the base space, and its spikes are fibers above points of the sphere. The Hopf fibration will also have the 2-sphere as the base space, the fibers will be circles (not necessarily glued to the base space), but the topology of the total space will be less trivial. An important nontrivial example is a Möbius band as the total space (see also Shoemake (1994)), with the central circle as the base space, and fibers being the twisting line segments along the circle. The projection maps each point of the Möbius band on a line segment to its point on the central circle, and the inverse image of a point on the central circle is the whole line segment (Fig. 3). Finally, the Hopf fibration is a mapping from a 3-sphere — the

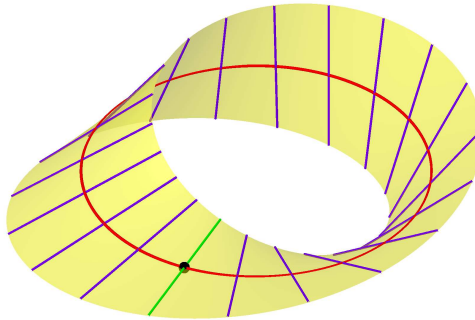


Fig. 3: Möbius band with the central circle as the base space and segments as fibers. Each segment is projected to its point of intersection with the central circle.

total space  $\mathcal{T}^3$  (the exponent indicates the dimension of the space) to a 2-sphere — the base space  $\mathcal{B}^2$  such that each distinct circle — fiber, on the 3-sphere  $\mathcal{T}^3$  corresponds to a distinct point on the 2-sphere  $\mathcal{B}^2$ . Oppositely, the total space  $\mathcal{T}^3$  is formed by circular fibers corresponding to all points on the base space — 2-sphere  $\mathcal{B}^2$ . Furthermore, inverse images of points on the 2-sphere correspond to non-intersecting linked Villarceau circles on a torus in the 3-sphere when stereographically projected (Fig. 2).

The Hopf fibration's analytic definition in the coordinate geometry (expression (5)) is given in the following lines after some preliminary remarks. For an elementary introduction to the Hopf fibration with visualizations, see Lyons (2003); Treisman (2009); Ozols (2007), and for further details and proofs in modern topological language, see the textbook by Hatcher (2002), Chapter 4.

For the sake of visualization, we follow the direct construction of the Hopf fibration in the real four-dimensional space  $\mathbb{R}^4$ , for example, in Treisman (2009), and additionally, we give a complex alternative useful for simple calculations. Therefore, as a valuable by-product, we will obtain not only the visualization of objects embedded in  $\mathbb{R}^4$  but also

a visual interpretation in  $\mathbb{C}^2$ , where  $\mathbb{C}^2 = \mathbb{C} \times \mathbb{C}$  is the Cartesian product of two complex coordinate systems. With respect to the previous paragraph,  $\mathcal{T}^3$  will represent a 3-sphere and  $\mathcal{B}^2$  a 2-sphere.

**Analytic definition of the Hopf fibration.** At first, we construct a mapping that projects a point on  $\mathcal{T}^3$  to a point on  $\mathcal{B}^2$ . A unit 2-sphere  $\mathcal{B}^2$  in the real three-dimensional space  $\mathbb{R}^3$  is the set of points given by the equation

$$x^2 + y^2 + z^2 = 1. \quad (1)$$

A unit 3-sphere  $\mathcal{T}^3$  in  $\mathbb{R}^4$  is given by the analogical equation

$$x^2 + y^2 + z^2 + w^2 = 1. \quad (2)$$

Assuming complex numbers  $z_1 = x_0 + iy_0$  and  $z_2 = z_0 + iw_0$ , we identify  $\mathbb{C}$  with  $\mathbb{R}^2$  as  $z_1 = [x_0, y_0]$  and  $z_2 = [z_0, w_0]$ .<sup>4</sup> This way, the unit 3-sphere  $\mathcal{T}^3$  embedded in  $\mathbb{C}^2$  has the equation

$$|z_1|^2 + |z_2|^2 = 1. \quad (3)$$

Assuming a complex number  $\zeta = x_\zeta + iy_\zeta$ , we can reformulate equation (1) of  $\mathcal{B}^2$  embedded in  $\mathbb{C} \times \mathbb{R}$  as follows

$$|\zeta|^2 + z^2 = 1. \quad (4)$$

The mapping

$$\begin{aligned} f : \mathbb{C}^2 &\rightarrow \mathbb{C} \times \mathbb{R} \text{ such that} \\ f(z_1, z_2) &= (2z_1\overline{z_2}, |z_1|^2 - |z_2|^2) \end{aligned} \quad (5)$$

is called (*the Hopf fibration*).<sup>5</sup>

**Proposition 1.** For the image point  $[\zeta, z]$  on  $\mathcal{B}^2 \subset \mathbb{C} \times \mathbb{R}$ , its preimage  $[z_1, z_2]$  in the Hopf fibration (5) is on  $\mathcal{T}^3 \subset \mathbb{C}^2$ .

---

<sup>4</sup>The labeling  $x_0, y_0, z_0, w_0$  refers to the location of a point with respect to the coordinate axes  $x, y, z, w$ , which will be graphically interpreted later.

<sup>5</sup>At this point, the Hopf fibration is given existentially. Other equivalent definitions of the Hopf fibration as a ratio of complex numbers (see Hatcher (2002)), or via quaternions (see Hanson (2006)) would need much broader theoretical discourse and would not fit better to our perspective.



Substituting  $\zeta = 2z_1\overline{z_2}$  and  $z = |z_1|^2 - |z_2|^2$  into equation (4) it holds

$$\begin{aligned}
|2z_1\overline{z_2}|^2 + (|z_1|^2 - |z_2|^2)^2 &= 1 \\
4((z_1\overline{z_2})(\overline{z_1}z_2)) + |z_1|^4 - 2(z_1\overline{z_1})(z_2\overline{z_2}) + |z_2|^4 &= 1 \\
(|z_1|^2 + |z_2|^2)^2 &= 1 \\
\text{since } |z_1|^2 + |z_2|^2 \geq 0, \text{ we have } |z_1|^2 + |z_2|^2 &= 1.
\end{aligned} \tag{6}$$

According to equation (3), the point  $[z_1, z_2]$  lies on  $\mathcal{T}^3$ .

Next, we discuss how to create a circle from a point on  $\mathcal{T}^3$  such that its image is a fixed point on  $\mathcal{B}^2$ .

**Proposition 2.** The Hopf fibration (5) maps all points of a circular fiber on  $\mathcal{T}^3 \subset \mathbb{C}^2$  to one point on  $\mathcal{B}^2 \subset \mathbb{C} \times \mathbb{R}$ .

Let  $[z_1, z_2]$  be a point on 3-sphere  $\mathcal{T}^3 \in \mathbb{C}^2$ . Assume a complex number  $\lambda = l_1 + il_2 \in \mathbb{C}$  such that  $|\lambda|^2 = 1$ , i.e.  $\lambda$  represents a point on a unit circle embedded in  $\mathbb{C}$ . From equation (6) for the point  $[\lambda z_1, \lambda z_2] \in \mathbb{C}^2$ , it holds

$$|\lambda z_1|^2 + |\lambda z_2|^2 = |\lambda|^2(|z_1|^2 + |z_2|^2) = |z_1|^2 + |z_2|^2 = 1, \text{ for each } \lambda. \tag{7}$$

Hence the point  $[\lambda z_1, \lambda z_2]$  lies on  $\mathcal{T}^3 \subset \mathbb{C}^2$ .

Rewriting the point  $[\lambda z_1, \lambda z_2] \in \mathbb{C}^2$  to its parametric representation in  $\mathbb{R}^4$  with  $\lambda = l_1 + il_2$ ,  $z_1 = x_0 + iy_0$  and  $z_2 = z_0 + iw_0$ , we have

$$\begin{pmatrix} \text{Re}(\lambda z_1) \\ \text{Im}(\lambda z_1) \\ \text{Re}(\lambda z_2) \\ \text{Im}(\lambda z_2) \end{pmatrix} = \begin{pmatrix} l_1 x_0 - l_2 y_0 \\ l_1 y_0 + l_2 x_0 \\ l_1 z_0 - l_2 w_0 \\ l_1 w_0 + l_2 z_0 \end{pmatrix}. \tag{8}$$

For each  $[l_1, l_2] \in \mathbb{R}^2$ , the last expression defines a set of points  $l_1 \vec{u} + l_2 \vec{v}$  in a plane in  $\mathbb{R}^4$  through the origin  $O = [0, 0, 0, 0]$  with the directional vectors  $\vec{u} = (x_0, y_0, z_0, w_0)$  and  $\vec{v} = (-y_0, x_0, -w_0, z_0)$ . Considering equation (7), the set of all points  $[\lambda z_1, \lambda z_2]$  for each  $\lambda$  is the intersection of  $\mathcal{T}^3$  and a plane through its center. Hence the set of all points  $[\lambda z_1, \lambda z_2]$  for  $\lambda \in \mathbb{C}$  is a unit circle on  $\mathcal{T}^3$ .

From expression (5),  $f$  maps  $[\lambda z_1, \lambda z_2]$  for  $|\lambda|^2 = 1$

$$\begin{aligned}
f(\lambda z_1, \lambda z_2) &= (2\lambda z_1 \overline{\lambda z_2}, |\lambda z_1|^2 - |\lambda z_2|^2) = (2|\lambda|^2 z_1 \overline{z_2}, |\lambda|^2(|z_1|^2 - |z_2|^2)) \\
&= (2z_1 \overline{z_2}, |z_1|^2 - |z_2|^2) = f(z_1, z_2).
\end{aligned} \tag{9}$$

to the same point on the unit 2-sphere  $\mathcal{B}^2$  as  $[z_1, z_2]$ .

**Hopf coordinates.** In our synthetic reconstruction, we construct the inverse mapping — for a point on  $\mathcal{B}^2$ , we find the circle on  $\mathcal{T}^3$ . The point on  $\mathcal{B}^2$  will be constructed through its angles apparent in the representation of  $\mathcal{B}^2$  via its spherical coordinates. Therefore, we will find a relation between the spherical coordinates of a point on  $\mathcal{B}^2$  and a point  $[z_1, z_2]$  on  $\mathcal{T}^3$  in the trigonometric representation  $z_1 = r_A(\cos \alpha + i \sin \alpha)$  and  $z_2 = r_B(\cos \beta + i \sin \beta)$  for  $r_A, r_B \geq 0$  and  $\alpha, \beta \in \mathbb{R}$ . From equation (6), for a point  $[z_1, z_2]$  on  $\mathcal{T}^3$  it holds that  $|z_1|^2 + |z_2|^2 = r_A^2 + r_B^2 = 1$ , and so there exist a unique  $\gamma \in \langle 0, \frac{\pi}{2} \rangle$  such that  $r_A = \cos \gamma$  and  $r_B = \sin \gamma$ . Then a point on  $\mathcal{T}^3$  have the following coordinates in  $\mathbb{R}^4$

$$\begin{pmatrix} \cos \gamma \cos \alpha \\ \cos \gamma \sin \alpha \\ \sin \gamma \cos \beta \\ \sin \gamma \sin \beta \end{pmatrix}, \alpha, \beta \in \langle 0, 2\pi \rangle, \gamma \in \left\langle 0, \frac{\pi}{2} \right\rangle. \quad (10)$$

With the use of this representation, the image  $f(z_1, z_2)$  of the point  $[z_1, z_2]$  in the Hopf fibration (5) has the first coordinate

$$\begin{aligned} 2z_1 \overline{z_2} &= 2 \cos \gamma (\cos \alpha + i \sin \alpha) \sin \gamma (\cos \beta - i \sin \beta) = \\ &= 2 \cos \gamma \sin \gamma (\cos \alpha \cos \beta + \sin \alpha \sin \beta + \\ &+ i(\sin \alpha \cos \beta - \cos \alpha \sin \beta)) = \sin(2\gamma)(\cos(\alpha - \beta) + i \sin(\alpha - \beta)), \end{aligned} \quad (11)$$

and the second coordinate

$$|z_1|^2 - |z_2|^2 = r_A^2 - r_B^2 = \cos^2 \gamma - \sin^2 \gamma = \cos(2\gamma). \quad (12)$$

Let  $2\gamma = \psi \in \langle 0, \pi \rangle$  and  $\alpha - \beta = \varphi \in \langle 0, 2\pi \rangle$  (assuming mod  $2\pi$ , and also for all further operations with angles). Considering the real and imaginary parts in (11) and the third coordinate in (12), the coordinates of the image  $f(z_1, z_2)$  in  $\mathbb{R}^3$  are

$$\begin{pmatrix} \sin(2\gamma) \cos(\alpha - \beta) \\ \sin(2\gamma) \sin(\alpha - \beta) \\ \cos(2\gamma) \end{pmatrix} = \begin{pmatrix} \sin \psi \cos \varphi \\ \sin \psi \sin \varphi \\ \cos \psi \end{pmatrix}, \quad (13)$$

$$\psi \in \langle 0, \pi \rangle, \varphi \in \langle 0, 2\pi \rangle.$$

These are obviously the spherical coordinates of the image on the unit 2-sphere  $\mathcal{B}^2$ , and we have also reduced the number of parameters (from three  $\alpha, \beta, \gamma$  to two  $\varphi, \psi$ ). Finally, to construct the preimage point from its image, we substitute  $\varphi$  and  $\psi$  to its equation

(10) on  $\mathcal{T}^3$  in  $\mathbb{R}^4$  obtaining the so-called *Hopf coordinates of a 3-sphere*

$$\begin{pmatrix} \cos \frac{\psi}{2} \cos(\varphi + \beta) \\ \cos \frac{\psi}{2} \sin(\varphi + \beta) \\ \sin \frac{\psi}{2} \cos \beta \\ \sin \frac{\psi}{2} \sin \beta \end{pmatrix}, \beta, \varphi \in \langle 0, 2\pi \rangle, \psi \in \langle 0, \pi \rangle. \quad (14)$$

Represented in  $\mathbb{C}^2$ , we have

$$\begin{pmatrix} z_1 \\ z_2 \end{pmatrix} = \begin{pmatrix} \cos \frac{\psi}{2} (\cos(\varphi + \beta) + i \sin(\varphi + \beta)) \\ \sin \frac{\psi}{2} (\cos \beta + i \sin \beta) \end{pmatrix}. \quad (15)$$

Let us show that two fibers are disjoint (see also in Treisman (2009)).

**Proposition 3.** Hopf fibers are disjoint circles.

Let  $\mathcal{T}^3$  be a 3-sphere given by equation (2). Its intersection with the 3-space  $w = 0$  is the (equatorial) 2-sphere  $\mathcal{B}^2$  with the equation (1).

Consider a point  $A$  on  $\mathcal{T}^3$  with coordinates  $A[1, 0, 0, 0]$  in  $\mathbb{R}^4$ . The set of points  $c_A = \lambda_A A$  for  $|\lambda_A|^2 = 1, \lambda_A \in \mathbb{C}$  is the unit circle defined by the rotation of  $A$  by  $\lambda_A$  about the origin in the plane  $(x, y)$ . Now let us have another point  $B[x_B, y_B, z_B, w_B]$  on  $\mathcal{T}^3$  and not on  $c_A$  through  $A$ , hence  $(z_B, w_B) \neq (0, 0)$ . The set of points  $c_B = \lambda_B B$  for  $|\lambda_B|^2 = 1, \lambda_B \in \mathbb{C}$  is, with respect to equation (7), a unit circle on  $\mathcal{T}^3$  with parametric representation

$$\begin{pmatrix} \operatorname{Re}(\lambda_B \sqrt{x_B^2 + y_B^2} (x_B + iy_B)) \\ \operatorname{Im}(\lambda_B \sqrt{x_B^2 + y_B^2} (x_B + iy_B)) \\ \operatorname{Re}(\lambda_B \sqrt{z_B^2 + w_B^2} (z_B + iw_B)) \\ \operatorname{Im}(\lambda_B \sqrt{z_B^2 + w_B^2} (z_B + iw_B)) \end{pmatrix}. \quad (16)$$

The unit circle  $c_B$  intersects the equatorial unit 2-sphere  $\mathcal{B}^2$  only if some point on  $c_B$  is in the 3-space  $w = 0$ . Let us again use the trigonometric representation to show that there are only 2 intersections of  $c_B$  with  $\mathcal{B}^2$  (such as great circles on a 2-sphere intersect its equator). Then  $z_B + iw_B = \sqrt{z_B^2 + w_B^2} (\cos \delta + i \sin \delta)$  for  $\delta \in \langle 0, 2\pi \rangle$ , and  $\lambda_B = \cos \varkappa + i \sin \varkappa$  for  $\varkappa \in \langle 0, 2\pi \rangle$ . For the point on  $c_B$  in the 3-space  $w = 0$  it holds

$$\begin{aligned} \operatorname{Im}(\lambda_B \sqrt{z_B^2 + w_B^2} (z_B + iw_B)) &= \operatorname{Im}((\cos \varkappa + i \sin \varkappa) (\sqrt{z_B^2 + w_B^2} (\cos \delta + i \sin \delta))) \\ &= \sqrt{z_B^2 + w_B^2} \sin(\varkappa + \delta) = 0 \end{aligned} \quad (17)$$

has, for  $(z_B, w_B) \neq (0, 0)$ , two solutions for  $\lambda_B$ :  $\varkappa = -\delta \pmod{2\pi}$  or  $\varkappa = \pi - \delta \pmod{2\pi}$

for each  $\delta \in \langle 0, 2\pi \rangle$ . Therefore,  $c_B$  has only two antipodal points  $K_1$  and  $K_2$  in common with  $\mathcal{B}^2$ .

Since for  $z$ -coordinates of  $c_B$  we have

$$\begin{aligned} \operatorname{Re}((\cos \varkappa + i \sin \varkappa)(\sqrt{z_B^2 + w_B^2}(\cos \delta + i \sin \delta))) &= \sqrt{z_B^2 + w_B^2} \cos(\varkappa + \delta) \neq 0 \\ &\text{for } \varkappa = -\delta \text{ or } \varkappa = \pi - \delta, \end{aligned} \quad (18)$$

the points  $K_1$  and  $K_2$  on the circle  $c_B$  are not in the plane  $(x, y)$ . Hence, the circles  $c_A$  and  $c_B$ , which are circular fibres in the Hopf fibration are disjoint.

Without loss of generality, we can rotate any circular fibre of the unit 3-sphere  $\mathcal{T}^3$  into the position of  $c_A$  and so all circular fibers on  $\mathcal{T}^3$  are disjoint.

**Stereographic projection.** A reasonable choice to create a map of an ordinary 2-sphere (e.g., a map of a reference sphere of the Earth) is to perform its stereographic projection from the North pole onto a tangent plane at the South pole. Despite the distortion of lengths, the measure of angles is preserved (conformal mapping). As a result, circles on the 2-sphere not passing through the North pole are projected to circles, and circles through the North pole become lines. In our analogical four-dimensional case, each point of  $\mathcal{T}^3$  is projected via projecting rays through its fixed point – the center of projection, onto a 3-space touching  $\mathcal{T}^3$  in the antipodal point. Due to the conformity, in a stereographic projection of  $\mathcal{T}^3$  to a 3-space, all the circular Hopf fibers are projected to circles apart from the fiber through the center of projection, which projects to a line. We have already shown that the inverse images of points on  $\mathcal{B}^2$  in the Hopf fibration are disjoint circles. Moreover, in the stereographic projection, these disjoint fibers are projected onto linked circles (or a line) (see Lyons (2003)). Assuming a circle on  $\mathcal{B}^2$ , its inverse image in the Hopf fibration projects to a family of disjoint circles on  $\mathcal{T}^3$ , and these are projected in the stereographic projection to a torus. Consequently, the stereographic images of all the fibers create nested tori, see Tsai (2006) for Lun-Yi Tsai's exquisite artistic geometric illustrations.

## 3 Preliminary constructions

### 3.1 Double orthogonal projection

The double orthogonal projection of the 4-space onto two mutually perpendicular 3-spaces is a generalization of Monge's projection of an object into two mutually perpendicular planes (see Zamboj (2018a)). Let us briefly describe the orthogonal projection of a 2-sphere into a plane in order to understand the following double orthogonal projection of a 3-sphere into two mutually perpendicular 3-spaces.

In an orthogonal projection, the contour generator of a 2-sphere is a great circle — the intersection of the polar plane of the infinite viewpoint with respect to the 2-sphere (i.e., the plane perpendicular to the direction of the projection through the center of the 2-sphere) and the given 2-sphere. The apparent contour of the 2-sphere is also a circle — the orthogonal projection of the contour generator into the plane of projection (Fig. 4). Therefore, in the three-dimensional case of Monge's projection, we project a 2-sphere  $\gamma$  to disks  $\gamma_1$  and  $\gamma'_2$  in two perpendicular planes  $(x, z)$  and  $(x, y')$ . Then the plane  $(x, y')$  is rotated about the  $x$ -axis into the plane  $(x, z)$  (drawing plane) such that the  $y'$ -axis is rotated into the  $y$ -axis overlapping the  $z$ -axis but with the opposite orientation. Any point  $P$  in the 3-space  $(x, y, z)$  is projected orthogonally via its projecting rays to the conjugated image points  $P_1$  (front view) and  $P_2$  (top view after the rotation). The images of projecting rays of  $P$  become overlapping line through  $P_1$  and  $P_2$ , called the ordinal line (or line of recall) of  $P$ , and it is perpendicular to the  $x$ -axis in the drawing plane.

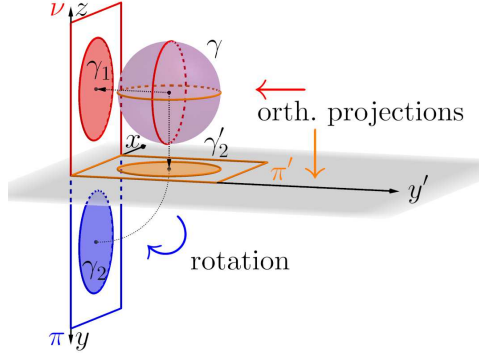


Fig. 4: Double orthogonal projection of a 2-sphere  $\gamma$  onto the disk  $\gamma_1$  in the 2-space  $\nu(x, z)$  and onto the disk  $\gamma'_2$  in the 2-space  $\pi'(x, y')$  rotated to  $\gamma_2$  in  $\pi(x, y)$  about the  $x$ -axis.

In analogy, let us have a 3-sphere in the 4-space (Fig. 5). We project it orthogonally into a 3-space. The contour generator on the 3-sphere is a 2-sphere — the intersection of the polar space of the infinite viewpoint with respect to the 3-sphere (i.e. the 3-space perpendicular to the direction of the projection through the center of the 3-sphere) and the given 3-sphere. The apparent contour of the 3-sphere is a 2-sphere — the orthogonal projection of the contour generator (2-sphere) into the 3-space of projection. Thus, in the double orthogonal projection both apparent contours in the 3-spaces  $\Xi(x, y, z)$  and  $\Omega'(x, z, w')$  of the 3-sphere  $\Gamma$ , are 2-spheres  $\Gamma_1$  and  $\Gamma'_2$ , respectively. Then we rotate  $\Omega'(x, z, w')$  about the plane  $\pi(x, z)$  into the 3-space  $\Xi(x, y, z)$  (modeling 3-space), such that the  $w'$ -axis is rotated to the  $w$ -axis overlapping the  $y$ -axis but with the opposite orientation. After the rotation, we say that  $\Gamma$  has two conjugated images in the modeling 3-space — the  $\Xi$ -image  $\Gamma_1$  and the  $\Omega$ -image  $\Gamma_2$  (rotated  $\Gamma'_2$ ).

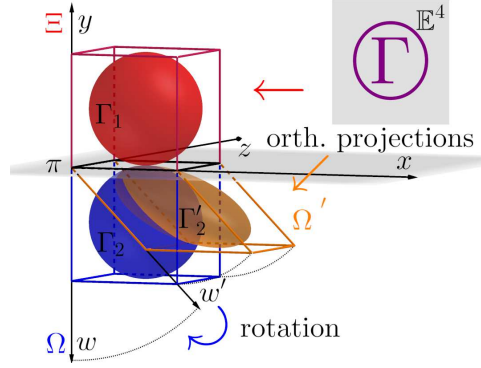


Fig. 5: Apparent contours of a 3-sphere  $\Gamma$  in the double orthogonal projection. The 2-sphere  $\Gamma_1$  in the 3-space  $\Xi(x, y, z)$  and the 2-sphere  $\Gamma'_2$  in the 3-space  $\Omega'(x, z, w')$  rotated to  $\Gamma_2$  in  $\Omega(x, z, w)$  about the plane  $\pi(x, z)$ .

### 3.2 Visualization of a point in $\mathbb{R}^4$ and $\mathbb{C}^2$

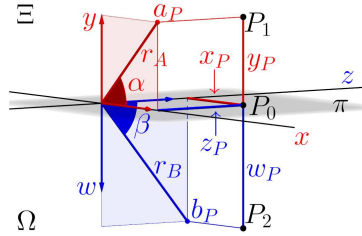


Fig. 6: Conjugated images  $P_1, P_2$  of a point  $P(x_P, y_P, z_P, w_P)$  in the double orthogonal projection, and visualization of the complex coordinates of  $P$ .

A point in the 4-space is given by its two conjugated images ( $\Xi$  and  $\Omega$ -image) lying on their common ordinal line, i.e. the line of overlapping rays of projection after the rotation in the modeling 3-space perpendicular to  $\pi(x, z)$ . Oppositely, let us have a point  $P$  with coordinates  $[x_P, y_P, z_P, w_P]$  in  $\mathbb{R}^4$ . The  $\Xi$ -image  $P_1[x_P, y_P, z_P]$  and  $\Omega$ -image  $P_2[x_P, z_P, w_P]$  are synthetically constructed in Fig. 6 using true lengths on the coordinate axes.<sup>6</sup> The ordinal line of the point  $P$  is perpendicular to  $\pi(x, z)$  through  $P_1$  and  $P_2$ . Moreover, if we interpret the point  $P$  to be in  $\mathbb{C}^2$  with coordinates  $P[a_P, b_P]$ , then  $a_P = [x_P, y_P]$  is on the complex line generated by the real axes  $x, y$ , and  $b_P = [z_P, w_P]$  is on another complex line given by  $z, w$ . Using the trigonometric representation, we have  $a_P = [r_A \cos \alpha, r_A \sin \alpha]$  and  $b_P = [r_B \cos \beta, r_B \sin \beta]$  (cf. equation (10)).

<sup>6</sup>Concretely, in the modeling 3-space with the orthogonal coordinate system  $(x, y, z)$  given in Fig. 6, we should say that the images of  $P$  have coordinates  $P_1[x_P, y_P, z_P]$  and  $P_2[x_P, -w_P, z_P]$ . Such coordinates would naturally be used for the implementation, if we wanted to construct the images from the parametric representation.

### 3.3 Visualization of a point on a 3-sphere

In an orthogonal projection of a 2-sphere into a plane, the points on the 2-sphere are projected to a disk. To show the position of some point in the image, we can draw its circle of latitude (in a plane perpendicular to the direction of the projection). Analogically, when we orthogonally project a 3-sphere into a 3-space, we can locate a point on the 3-sphere by drawing its “2-sphere of latitude” (in a 3-space perpendicular to the direction of the projection). In Monge’s projection, planes parallel to the plane  $(x, z)$  intersect the plane  $(x, y)$  in lines parallel to  $x$ . The sections of a 2-sphere with planes parallel to  $(x, z)$  in the Monge’s projection are indicated in Fig. 7a, and they create line segments in the top view and circles in their true size in the front view. In other words, if we imagine a 2-sphere passing orthogonally through a plane, their common intersection will be the tangent point extending continuously to the great circle and shrinking back to a point. Analogically, the 3-spaces parallel to the 3-space  $\Xi(x, y, z)$  intersect the 3-space  $\Omega(x, z, w)$  in planes parallel to  $\pi(x, z)$ . If a 3-sphere passes orthogonally through a 3-space, their common intersection is the tangent point, extending to the great 2-sphere and shrinking back to a point. Therefore, the intersections of the 3-sphere with a bundle of 3-spaces parallel to  $\Xi(x, y, z)$  are 2-spheres (Fig. 7b). Their  $\Xi$ -images are circles and  $\Omega$ -images are 2-spheres in the true size. This construction should give us some insight into the visualization of points on tori inside a 3-sphere that will be carried out later.

Let us have a point  $P$  on a 3-sphere  $\Gamma$  (Fig. 8, Suppl. File 1). The point  $P$  lies on some 2-sphere  $\sigma$  in a 3-space  $\Sigma$  parallel to  $\Xi(x, y, z)$ . Since  $\Sigma$  has the same  $w$ -coordinate as  $P$ , its  $\Omega$ -image appears as the plane  $\omega_2^\Sigma$  through  $P_2$  parallel to  $\pi(x, z)$ . The intersection of  $\omega_2^\Sigma$  and  $\Gamma_2$  is a circle  $\sigma_2$  that is the boundary of the  $\Omega$ -image of  $\sigma$ . The  $\Xi$ -image  $\sigma_1$  through  $P_1$  is a 2-sphere concentric with  $\Gamma_1$  and the radius equal to the radius of  $\sigma_2$ .

### 3.4 Stereographic projection of a point on a 3-sphere into a 3-space

Let us have a unit 3-sphere  $\Gamma$  with the center  $S = [0, 1, 0, 1]$  (cf. equation (2))

$$x^2 + (y - 1)^2 + z^2 + (w - 1)^2 = 1. \quad (19)$$

We project points of the 3-sphere  $\Gamma$  from its point  $N = [0, 2, 0, 1]$  onto the 3-space  $\Omega(x, z, w) : y = 0$  that touches  $\Gamma$  at the antipodal point  $M = [0, 0, 0, 1]$ . Let us have a point  $P$  on  $\Gamma$  with its images  $P_1$  and  $P_2$  (Fig. 9, Suppl. File 2). The stereographic image  $P_S$  of the point  $P$  in  $\Omega(x, z, w)$  is the intersection of the line  $NP$  and  $\Omega(x, z, w)$ . The line  $N_1P_1$  intersects  $\pi(x, z)$  in the point  $P_{S_1}$ . The intersection of the ordinal line through  $P_{S_1}$  and the  $\Omega$ -image  $N_2P_2$  is the desired point  $P_{S_2}$  that coincides with  $P_S$  in the 4-space.

Since stereographic projection is a conformal mapping, we can also conveniently

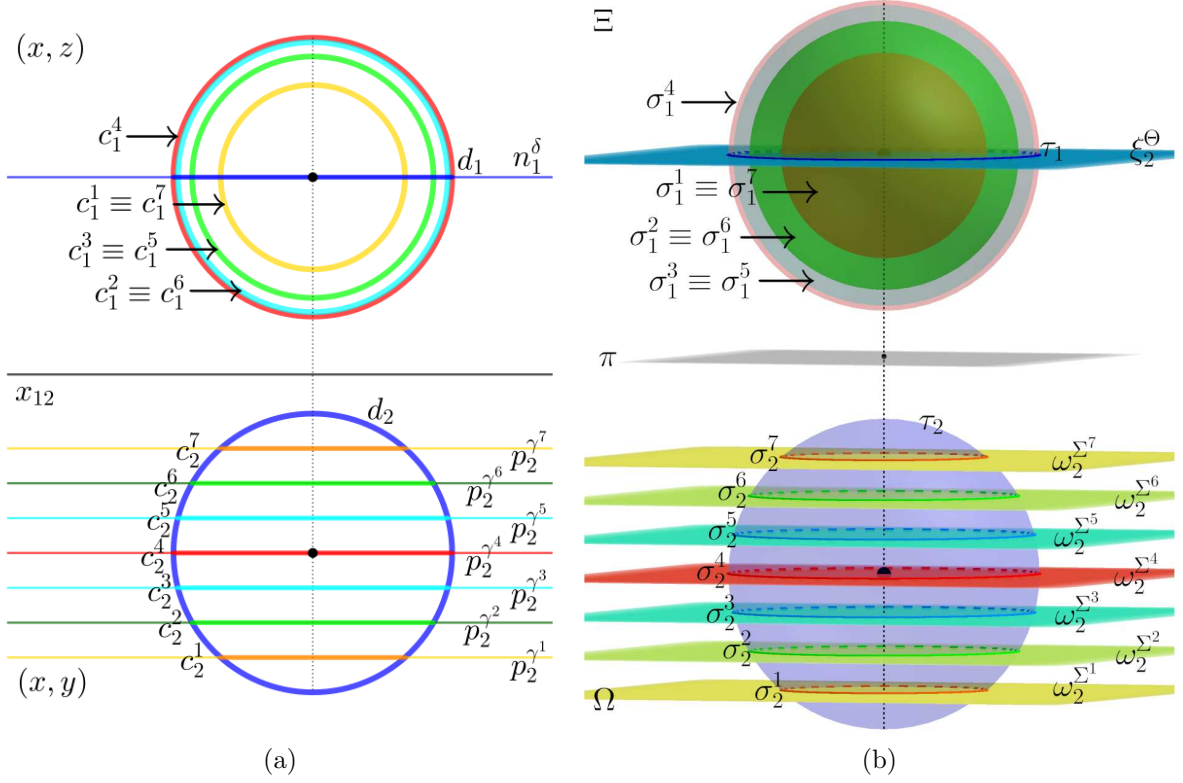


Fig. 7: (a) Circular sections  $c^1, \dots, c^7$  of a 2-sphere with planes  $\gamma^1, \dots, \gamma^7$  parallel to  $(x, z)$  in Monge's projection. The planes are given by their intersections  $p^\gamma$  with the plane  $(x, y)$ . The apparent contours of the sections are circles  $c_1^1, \dots, c_1^7$  in the front view and segments  $c_2^1, \dots, c_2^7$  in the top view. (b) Sections  $\sigma^1, \dots, \sigma^7$  of a 3-sphere with 3-spaces  $\Sigma^1, \dots, \Sigma^7$  parallel to the 3-space  $\Xi(x, y, z)$  are 2-spheres. The 3-spaces are given by their intersections  $\omega^\Sigma$  with the 3-space  $\Omega$ . The  $\Xi$ -images  $\sigma_1^1, \dots, \sigma_1^7$  of the spherical sections are 2-spheres in the true shape and  $\Omega$ -images  $\sigma_2^1, \dots, \sigma_2^7$  are disks.

project the 2-sphere  $\sigma$  through the point  $P$  described in the previous section. The stereographic image  $\sigma_S$  of the 2-sphere  $\sigma$  is a 2-sphere  $\sigma_S$  with the center  $G_S$  on the ordinal line through the center  $S_1$  of  $\sigma_1$ . Its equatorial circle  $g_S$  is the image of the tangent circle  $g_1$  on the sphere  $\Gamma_1$  of the cone with the vertex  $N_1$ , i.e. the intersection of the polar plane of the pole  $N_1$  with respect to  $\sigma_1$  and  $\sigma_1$ . Therefore, with the use of some point on  $g_1$ , we construct the image circle  $g_S$  of the circle  $g$ , and the center  $G_S$  of  $g_S$  is the center of the 2-sphere  $\sigma_S$  — the stereographic image of the 2-sphere  $\sigma$ .

## 4 Synthetic construction of a Hopf fiber

In this section, we extract important properties from the introductory mathematical background and find them geometrically in images of the double orthogonal projection. This way, we synthetically construct a circular fiber on a 3-sphere from a point on a 2-sphere with elementary geometric constructions and liberate it from the analytic description.



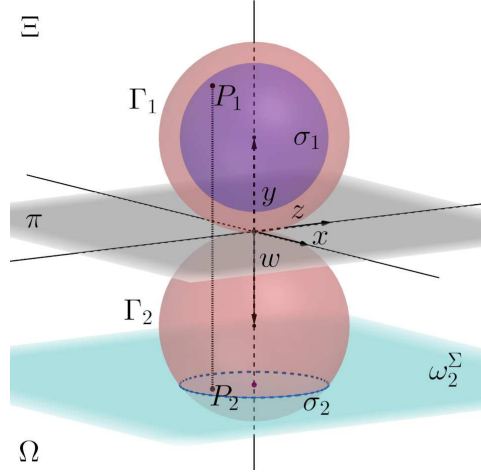


Fig. 8: Conjugated images  $P_1$  and  $P_2$  of a point  $P$  on the spherical section  $\sigma$  of a 3-sphere  $\Gamma$  with a 3-space  $\Sigma$  parallel to  $\Xi(x, y, z)$ . The  $\Xi$ -image  $P_1$  is on  $\sigma_1$ , which is in its true shape. The  $\Omega$ -image  $\sigma_2$  of the 2-sphere  $\sigma$  is a disk with the same radius as  $\sigma_1$ . The  $\Omega$ -image  $P_2$  lies on the disk  $\sigma_2$ .

In the interactive 3D model <https://www.geogebra.org/m/yt27evc8> (or Suppl. File 1), the user can manipulate the position of  $P_1$  on  $\sigma_1$  and  $\omega_2^\Sigma$  with the “Moving point” on the  $w$ -axis and observe the conjugated images of positions of the point  $P$  on the 3-sphere.

Whereas for the computations we used the equations of a 3-sphere  $\mathcal{T}^3$  with the center in the origin, for the sake of visualization (to differentiate the  $\Xi$  and  $\Omega$ -images), it is more suitable to use a 3-sphere  $\mathcal{T}^3$  with the center  $[0, 1, 0, 1]$ . Then the 2-sphere  $\mathcal{B}^2$  has the center with the coordinates  $[0, 1, 0]$  in  $\Xi(x, y, z)$ . Such translation does not influence the properties of the Hopf fibration. This applies for Figs. 10–12, 14–18 and the parametric equations corresponding to the visualizations are in Appendix.

Let  $Q \in \Xi(x, y, z)$  be an arbitrary point on  $\mathcal{B}^2$  (Fig. 10, Suppl. File 3). We will find its Hopf fiber — circle  $c$  on  $\mathcal{T}^3$ . Equations (13), 25 and (14,26) show a relation between the spherical coordinates of the point  $Q$  (with parameters  $\varphi$  and  $\psi$ ) and Hopf coordinates of the fiber  $c$  (with parameters  $\varphi, \psi$  and  $\beta$ ). The construction proceeds in the following steps (see the step-by-step construction):

1. Construct any point  $Q$  on  $\mathcal{B}^2$ .
2. Find an angle  $\varphi$  (from equation (13)): Construct the plane parallel to  $(x, y)$  through  $Q$ , that cuts  $\mathcal{B}^2$  in a circle. The oriented angle between the radius parallel to the  $x$ -axis and the radius terminating in the point  $Q$  is the angle  $\varphi$ .
3. Construct an arbitrary angle  $\beta$  such that we can graphically add it to  $\varphi$ : First, translate  $\varphi$  to  $\varphi'$  in the plane  $(x, y)$  with its vertex in the center of  $\mathcal{B}^2$ , and the initial side in the direction of the non-negative  $x$ -axis. Now choose  $\beta$  with the same vertex and initial side in the terminal side of  $\varphi'$ . For implementation, it is enough to choose  $\beta$  on the top semicircle, because the points  $P$  and  $P'$  constructed

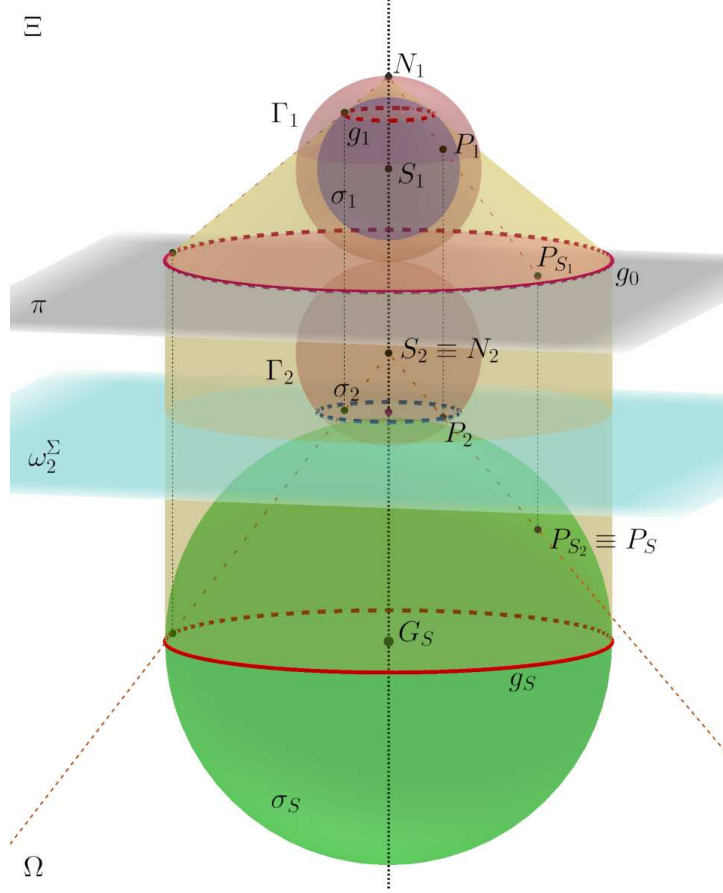


Fig. 9: The stereographic image  $P_S$  of a point  $P$  on a 3-sphere  $\Gamma$  projected from the center  $N$  to the tangent 3-space  $\Omega(x, z, w)$ . The stereographic image  $P_S$  lies in the 3-space  $\Omega$  hence it is also the  $\Omega$ -image  $P_{S_2}$  constructed as the intersection of  $NP$  and  $\Omega$ . Additionally, the spherical section  $\sigma$  from Fig. 8 is stereographically projected to the 2-sphere  $\sigma_S$ . For analytic coordinates of  $P_S$  see equation (27).

In the interactive 3D model <https://www.geogebra.org/m/xth6uszb> (or Suppl. File 2), the user can, again, manipulate  $P_1$  on  $\sigma_1$  and  $\omega_2^\Sigma$  by “Moving point” on  $w$ -axis and observe the stereographic images.

in step 7) dependent on  $\beta$  will be antipodal. Additionally, construct  $\alpha$  such that  $\alpha = \varphi' + \beta$  (cf. equation (13)). The angles  $\alpha$  and  $\beta$  are arguments of some complex points  $a_P = [r_A \cos \alpha, r_A \sin \alpha] \in (x, y)$  and  $b_P = [r_B \cos \beta, r_B \sin \beta] \in (z, w)$  (see the derivation of  $z_1$  and  $z_2$  above equation (10)).

4. Find an angle  $\psi$  (from equation (13)): Construct the great circle of  $\mathcal{B}^2$  through  $Q$  with a diameter parallel to the  $x$ -axis. Choose a radius in the  $(y, z)$ -plane to be the initial side of the angle  $\psi$  with the terminal side being the radius through  $Q$ .
5. Construct the moduli of the points  $a_P$  and  $b_P$  (cf. equation (10)): Let  $\gamma$  be the half-angle of  $\psi$  and find its cosine by dropping a perpendicular to the initial side of  $\psi$ . The length  $\cos \frac{\psi}{2} = \cos \gamma$  is the modulus  $r_A$  of the point  $a_P$ . Similarly find the length  $\sin \frac{\psi}{2} = \sin \gamma$  on the radius in the direction of the  $x$ -axis, which is the

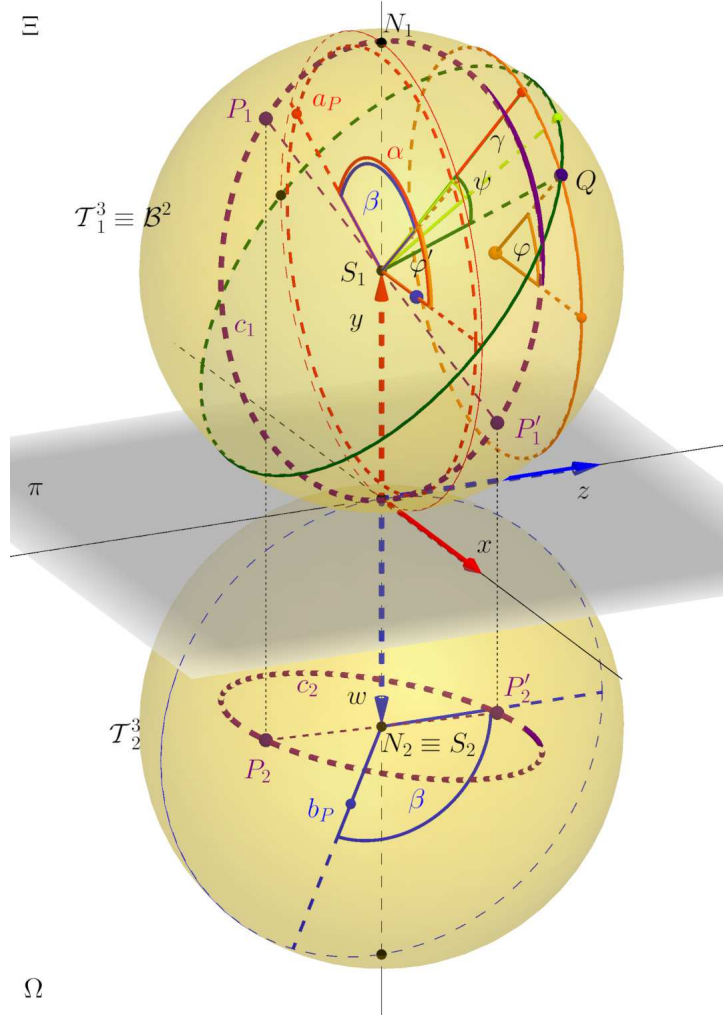


Fig. 10: Construction of the Hopf fiber  $c$  on  $\mathcal{T}^3$  corresponding to a point  $Q$  on  $\mathcal{B}^2$ . With the step-by-step construction <https://www.geogebra.org/m/w2kugajz> (or Suppl. File 3), the reader can follow the steps of the construction from the text in the *Construction Protocol* window. Use the arrows to move between the steps. From step 1), the user can move the point  $Q$  on  $\mathcal{B}^2$  and dynamically change all the dependent elements of the model and the resulting fiber. From step 3), the user can also manipulate the angle  $\beta$  and observe positions of the conjugated images of  $P$  and  $P'$  on the fiber. Steps 10 and 11 belong to the construction of the stereographic projection in Fig. 14.

modulus  $r_B$  of  $b_P$ .

6. Construct points  $a_P$  and  $b_P$ : Using the moduli and arguments of  $a_P$  and  $b_P$ , construct them according to Fig. 6.
7. Construct  $\Xi$  and  $\Omega$ -images of the point  $P$ : Having  $a_P$  and  $b_P$ , we finalize the images  $P_1$  and  $P_2$  on the parallels with the reference axes (as in Fig. 6).
8. Construct the antipodal point  $P'$  on  $\mathcal{B}^2$ : Parallel projection preserves the central symmetry, and the images  $P'_1$  and  $P'_2$  are the reflections of  $P_1$  and  $P_2$  about the centers  $S_1$  and  $S_2$  of the images of  $\mathcal{T}^3$ .

9. Construct the Hopf fiber corresponding to the point  $Q$ : The Hopf fiber is a circle  $c$  consisting of the locus of points  $P$  dependent on  $\beta$ . We have a point construction of  $P$ , which can be repeated for different choices of  $\beta$  even though, at this point, we comfortably use the GeoGebra tool to draw the locus. The orthogonal projections of  $c$  will appear as ellipses (or circles, or segments)  $c_1$  and  $c_2$ .

Manipulating with  $\beta$  in the interactive applet,  $P$  moves on its fiber  $c$ . Moving with  $Q \in \mathcal{B}^2$ , the whole fiber  $c$  moves on  $\mathcal{T}^3$ .

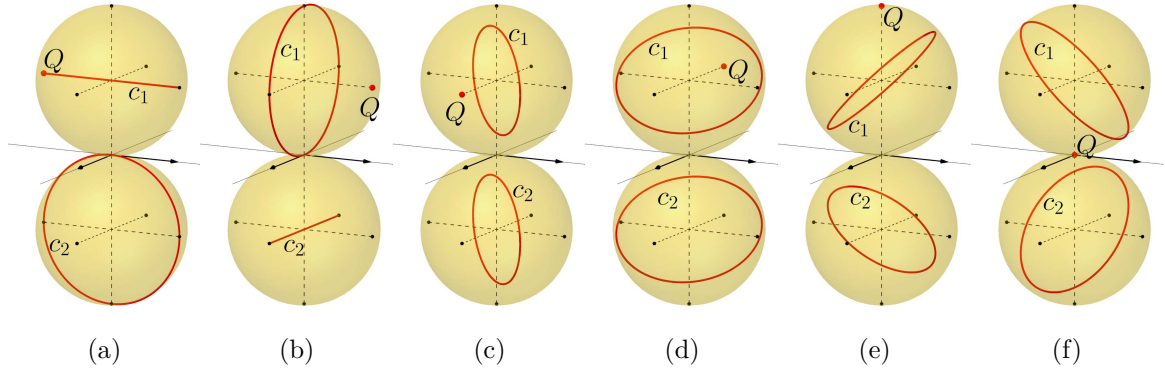


Fig. 11: Conjugated images of the fibers corresponding to the point  $Q$  in special positions: (a)  $Q=[0,1,-1]$ , (b)  $Q=[0,1,1]$ , (c)  $Q=[1,1,0]$ , (d)  $Q=[-1,1,0]$ , (e)  $Q=[0,2,0]$ , (f)  $Q=[0,0,0]$ .

Let us investigate images of the fibers corresponding to special points on the base sphere  $\mathcal{B}^2$  on diameters parallel to  $x, y$ , and  $z$  axes (Fig. 11).

(with respect to the translated coordinates of the centers of  $\mathcal{B}^2$  and  $\mathcal{T}^3$ )

(a), (b) The fibers of points  $[0, 1, \pm 1]$  or  $\varphi = 0$  and  $\psi = 0, \pi$  are in the planes  $(x, w)$  and  $(y, z)$ , respectively. Thus, their conjugated images are a segment and a great circle. Particularly, for  $\psi = \pi$ , the point on the base sphere lies on its fiber.

(c), (d) The fibers of points  $[\pm 1, 1, 0]$  or  $\varphi = 0, \pi$  and  $\psi = \frac{\pi}{2}$  lie in the plane of symmetry of  $x$  and  $z$  axes and their conjugated images are congruent.

(e), (f) The fibers of points  $[0, 1 \pm 1, 0]$  or  $\varphi = \frac{\pi}{2}, \frac{3\pi}{2}$  and  $\psi = \frac{\pi}{2}$  have their  $\Xi$ -images in the plane of symmetry of  $y$  and  $z$  axes and  $\Omega$ -images in the plane of symmetry of  $x$  and  $w$  axes.

We have already mentioned that fibers corresponding to two distinct points on the base 2-sphere  $\mathcal{B}^2$  create linked circles. Let us have two points  $Q$  and  $Q'$  on  $\mathcal{B}^2$  and their fibers  $c$  and  $c'$ , respectively. From the conjugated images of the fibers  $c$  and  $c'$ , we can easily observe that they are disjoint. Otherwise, if  $c$  and  $c'$  have an intersecting point  $R$ , their conjugated images  $c_1, c'_1$  and  $c_2, c'_2$  must intersect in the conjugated images  $R_1, R_2$  of the point  $R$ . In the case that the conjugated images of a fiber are in a plane perpendicular

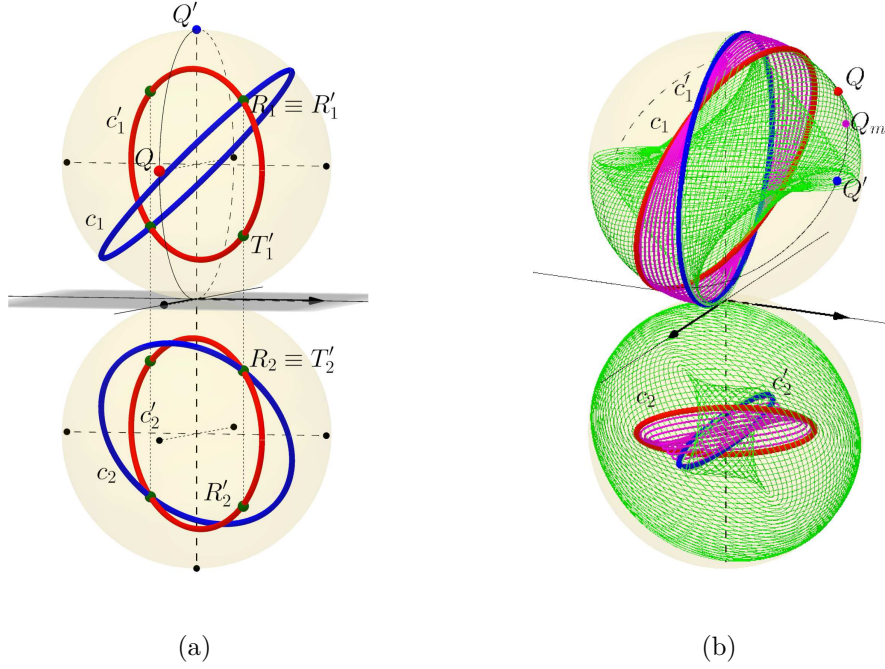


Fig. 12: (a) Special position of the points  $Q$  and  $Q'$  such that the conjugated images of disjoint fibers  $c$  and  $c'$  intersect. In the  $\Xi$ -image,  $c_1$  and  $c'_1$  intersect in a point  $R_1 \equiv R'_1$ , but their  $\Omega$ -images  $R_2 \in c_1$  and  $R'_2 \in c'_2$  are distinct. Similarly the point  $T'$  on  $c'$  has its  $\Omega$  image  $T'_2 \equiv R_2$ , but their  $\Xi$ -images are distinct. (b) Motion of the point  $Q_m$  between  $Q$  and  $Q'$ . The pink fibers correspond to positions of  $Q_m$  on the shorter arc between  $Q$  and  $Q'$ , the green fibers correspond to the motion of  $Q_m$  on the longer arc.

In the interactive model <https://www.geogebra.org/m/ebjkx8pj> (or Suppl. File 4), the user can with the scroll bars dynamically change the positions of  $Q$  and  $Q'$  dependant on parameters  $(\varphi, \psi)$  and  $(\varphi', \psi')$  (based on equation (25)), respectively. The point  $Q_m$  can move freely along the great circle through  $Q$  and  $Q'$ . The conjugated images of the fibers corresponding to  $Q_m$  draw their traces in the modeling 3-space.

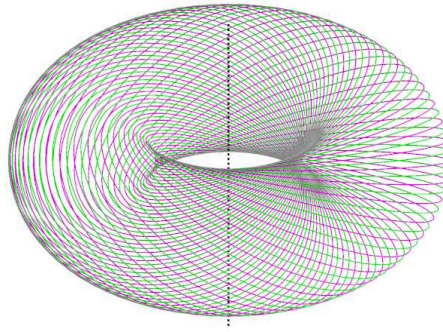


Fig. 13: A torus in a three-dimensional space generated by revolution of Villarceau circle. All the generating circles are interlinked.

to  $\pi$  (e.g., Fig. 12a), we must not swap the conjugated images of its points. Furthermore, we should more carefully say that the circles are linked on the 3-sphere  $\mathcal{T}^3$ , but this property cannot be validated in the embedding 4-space. Analogically, imagine a point

in a circular region on a 2-sphere embedded in a 3-space. On the 2-sphere, the point cannot escape the bounding circle. However, if we remove the 2-sphere and leave only the 3-space, the point is not bounded at all. Hence, to analyze the fibers' interlinkedness, we need to understand the topology of the underlying 3-sphere  $\mathcal{T}^3$ . Let us construct a great circle on  $\mathcal{B}^2$  through  $Q$  and  $Q'$  and observe the motion of the fiber of a point  $Q_m$  on the circle moving from  $Q$  to  $Q'$  (Fig. (12b)). During the motion, the moving fiber twists along some surface. In fact, the generating fibers are always one of a pair of Villarceau circles along a torus (cf. Fig. 13 with a 3-dimensional parallel projection of a torus generated by Villarceau circle into a plane). The toroidal structure of a 3-sphere will be more vivid in Section 5 with the use of a stereographic projection.

#### 4.1 Construction of the stereographic image of a Hopf fiber

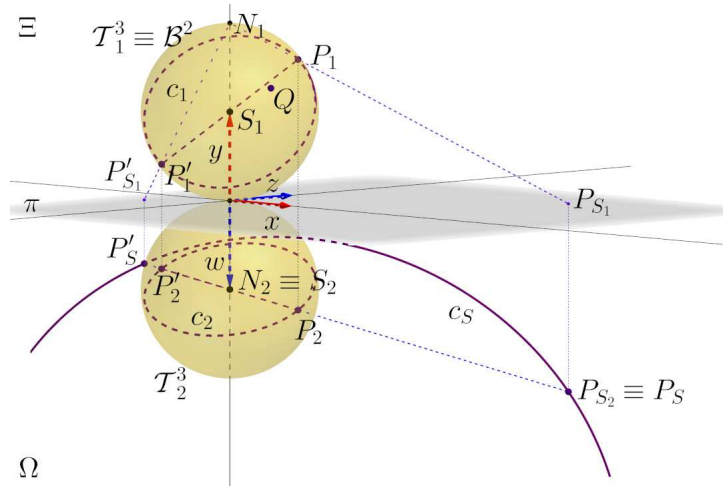


Fig. 14: Construction of the stereographic image  $c_S$  of the Hopf fiber  $c$  (cf. Fig. 9). The fiber  $c_S$  is constructed as the locus of points  $P_S$  and  $P'_S$  dependant on the angle  $\beta$ . Stereographic images are constructed in steps 10 and 11 in the step-by-step construction <https://www.geogebra.org/m/w2kugajz> (or Suppl. File 3) described in Fig. 10.

To grasp the circular structure of the Hopf fibration, we construct the fibers in stereographic projection. We use the same center of projection and antipodal tangent space  $\Omega(x, z, w)$  as in Section 3.4. Continuing from the previous construction:

10. Construct a stereographic image of the point  $P$ : Let  $N = [0, 2, 0, 1]$  be on  $\mathcal{T}^3$ , and the 3-space  $\Omega(x, z, w)$  tangent to  $\mathcal{T}^3$  at the point  $[0, 0, 0, 1]$ . The intersection of  $N_1P_1$  with  $\pi(x, z)$  is  $P_{S_1}$ . Dropping a perpendicular from  $P_{S_1}$  to the line  $N_2P_2$  gives us the point  $P_{S_2}$  that is also the true stereographic image  $P_S$ .
11. Construct a stereographic image of the fiber  $c$ : We use the locus tool from GeoGebra to construct a locus of points  $P_S$  dependent on the angle  $\beta$ . The stereographic image  $c_S$  of  $c$  is a circle or a line (if  $c$  passes through  $N$ ).



Again, manipulating with  $\beta$ ,  $P_S$  moves on  $c_S$ , and changing the position of  $Q \in \mathcal{B}^2$ , the circle  $c_s$  changes such that it may cover the whole modeling 3-space. In the following section, we show how to move with  $Q$  to obtain Hopf tori.

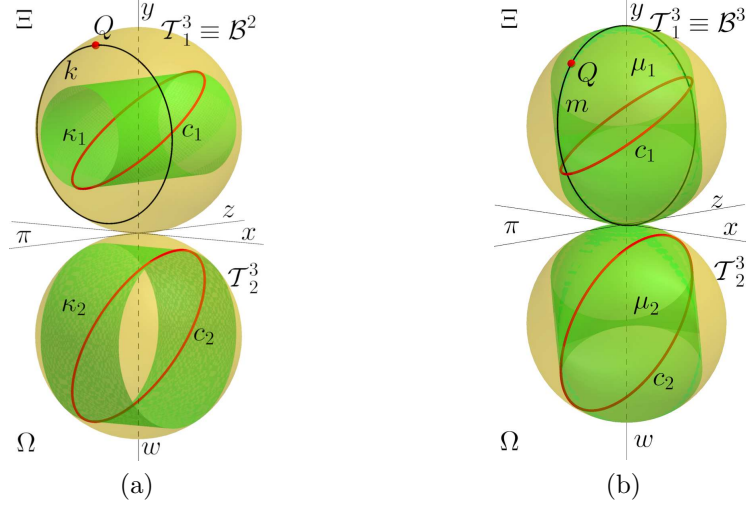


Fig. 15: (a) Torus  $\kappa$  on  $\mathcal{T}^3$  corresponding to a circle  $k$  on  $\mathcal{B}^2$  parallel to  $(x, y)$ -plane. The torus is generated by fibers  $c$  above points  $Q$  along the circle  $k$ . (b) Torus  $\mu$  on  $\mathcal{T}^3$  corresponding to a circle  $m$  on  $\mathcal{B}^2$  with a diameter parallel to  $z$ -axis. Again, the torus is generated by fibers  $c$  above points  $Q$  on  $m$ .

## 5 Hopf tori corresponding to circles on $\mathcal{B}^2$

The full exposition of the geometric nature of the Hopf fibration is apparent, when we visualize tori of Hopf fibers corresponding to circles on the base 2-sphere  $\mathcal{B}^2$ . With respect to the chosen stereographic projection, we divide the following constructions into two cases. First, we construct the tori on  $\mathcal{T}^3$  in  $\mathbb{R}^4(x, y, z, w)$  corresponding to circles on  $\mathcal{B}^2$  parallel with the plane  $(x, y)$  in the 3-space  $\Xi(x, y, z)$ , and then the tori on  $\mathcal{T}^3$  corresponding to circles on  $\mathcal{B}^2$  with the diameter parallel to  $z$ . Instead of point-by-point constructions, in the following interactive demonstrations (Suppl. Files 5 and 6), the objects are defined by their parametric representations (see equations (28) of the circle  $k$  on  $\mathcal{B}^2$ , (29) of the corresponding torus  $\kappa$ , (30) of the stereographic image of the torus  $\kappa$  in Appendix), and the user can manipulate with sliders of the angles  $\varphi$  and  $\psi$ .

### 5.1 Hopf torus of a circle parallel to $(x, y)$

Let us have a point  $Q$  on  $\mathcal{B}^2$  in  $\Xi(x, y, z)$  and a circle  $k$  parallel to  $(x, y)$  through the point  $Q$  (Fig. 15a, Suppl. File 5). From equation (13), we have the parametric coordinates of

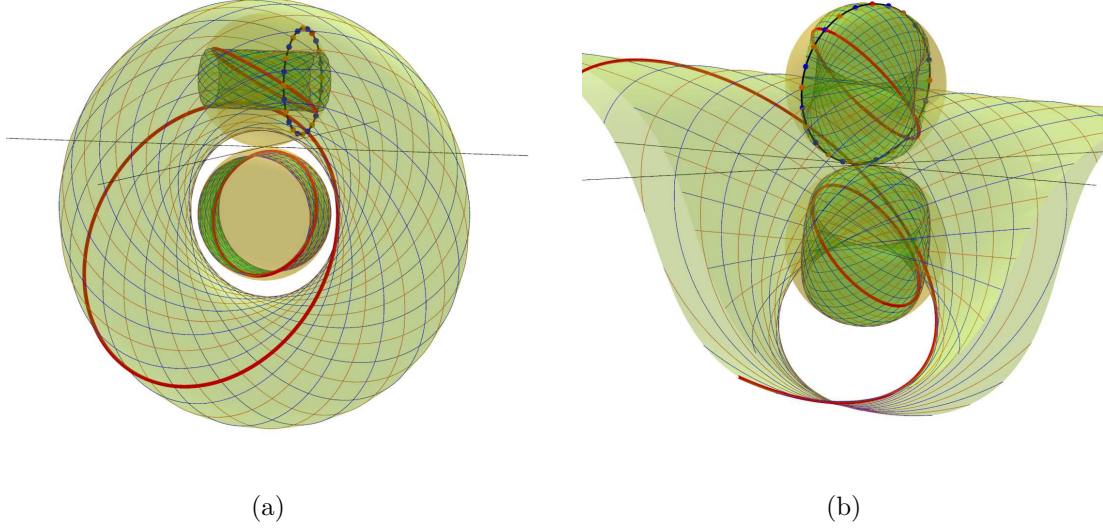


Fig. 16: (a) Blue and orange points on a circle on  $\mathcal{B}^2$  parallel to  $(x, y)$  and the corresponding family of circular fibers on  $\mathcal{T}^3$  generating a torus. The stereographic projection of this torus into  $\Omega(x, z, w)$  is a torus of revolution. (b) Blue and orange points on a circle on  $\mathcal{B}^2$  with a diameter parallel to  $z$ -axis and their fibers. One of the fibers pass through the center of stereographic projection, and so, its image is a line.

In the interactive models: (a) <https://www.geogebra.org/m/n4xg3sw6> (or Suppl. File 5), (b) <https://www.geogebra.org/m/vrasywpt> (or Suppl. File 6); the user can manipulate the spherical coordinates of  $Q$  from equation 25 and interactively change its circle on  $\mathcal{B}^2$  and the corresponding torus. The user can also turn off the visibility of the objects on  $\mathcal{B}^2$ , conjugated images in the double orthogonal projection, or the stereographic images.

points on the circle  $k$  given by the angle  $\varphi'$  for a fixed  $\psi$ :

$$k(\varphi') = \begin{pmatrix} \sin \psi \cos \varphi' \\ \sin \psi \sin \varphi' \\ \cos \psi \end{pmatrix}, \varphi' \in \langle 0, 2\pi \rangle. \quad (20)$$

Varying the angle  $\beta'$  (positions of  $P$  on  $c$ ) from equation (14) and the angle  $\varphi'$  (positions of  $Q$  on  $k$  corresponding to distinct fibers  $c$ ), we obtain the parametrization of a torus  $\kappa$  covered by the fibers on  $\mathcal{T}^3$ :

$$\kappa(\beta', \varphi') = \begin{pmatrix} \cos \frac{\psi}{2} \cos(\varphi' + \beta') \\ \cos \frac{\psi}{2} \sin(\varphi' + \beta') \\ \sin \frac{\psi}{2} \cos(\beta') \\ \sin \frac{\psi}{2} \sin(\beta') \end{pmatrix}, \beta', \varphi' \in \langle 0, 2\pi \rangle. \quad (21)$$



Fig. 16a shows the double orthogonal projection of the torus  $\kappa$  and its generating circles corresponding to points on the circle  $k$  with their stereographic images.

The conjugated images  $\kappa_1$  and  $\kappa_2$  of this torus are parts of cylindrical surfaces of revolution in  $\mathcal{T}_1^3$  and  $\mathcal{T}_2^3$ . This is a straightforward consequence of the relationship between the point  $Q$  and the angle  $\varphi'$ . From equation (21) with a fixed  $\psi$ , we obtain the  $\Xi$ -image  $\kappa_1$  as a part of a cylindrical surface of revolution about the axis parallel to  $z$  in the 3-space  $\Xi(x, y, z)$ . Similarly, the  $\Omega$ -image  $\kappa_2$  is a part of a cylindrical surface of revolution about the axis parallel to  $x$  in the 3-space  $\Omega(x, z, w)$ .

## 5.2 Hopf torus of a circle with diameter parallel to $z$

Let us have a point  $Q$  on  $\mathcal{B}^2$  and a circle  $m$  with a diameter parallel to  $z$  through the point  $Q$  (Fig. 15b, Suppl. File 6). The circle  $m$  has its parametric representation for a fixed angle  $\varphi$  and variable  $\psi'$  (from equation (13)):

$$m(\psi') = \begin{pmatrix} \sin \psi' \cos \varphi \\ \sin \psi' \sin \varphi \\ \cos \psi' \end{pmatrix}, \psi' \in \langle 0, \pi \rangle. \quad (22)$$

Varying the angle  $\psi'$  (positions of  $Q$  on  $m$ ), influences the moduli  $r'_A$  and  $r'_B$  of  $P$  on the corresponding fiber  $c$  (from equation (14)). More precisely,  $r'_A = \cos \gamma' = \cos \frac{\psi'}{2}$  and  $r'_B = \sin \gamma' = \sin \frac{\psi'}{2}$  with the fixed angle  $\varphi$  induce the family of non-intersecting circular fibers  $c(\beta')$  generating a torus:

$$\tau(\beta', \psi') = \begin{pmatrix} \cos \frac{\psi'}{2} \cos(\varphi + \beta') \\ \cos \frac{\psi'}{2} \sin(\varphi + \beta') \\ \sin \frac{\psi'}{2} \cos(\beta') \\ \sin \frac{\psi'}{2} \sin(\beta') \end{pmatrix}, \beta' \in \langle 0, 2\pi \rangle, \psi' \in \langle 0, \pi \rangle. \quad (23)$$

In contrast to the previous case, in which the torus  $\kappa$  was generated with the parameter  $\varphi$ , the torus  $\mu$  is generated with the parameter  $\psi$  interfering with all the coordinates. Therefore, the conjugated images of the torus  $\mu$  are more twisted. For the choice  $\psi' = 0$  and  $\beta' = \frac{\pi}{2} - \varphi$ , we always obtain the point  $[0, 1, 0, 0]$  lying on the torus  $\mu$ . This is the center  $N$  of the stereographic projection before the translation for visualization purposes, and hence, torus  $\mu$  always contains a point that is stereographically projected to infinity. Moreover, it contains a fiber through this point, too. The stereographic image of this fiber is a line. See Fig. 16b for the full exposition of the double orthogonal projection of the torus covered by its circles and their stereographic images. Let us have two tori  $\mu$  and  $\nu$  generated by great circles  $m$  and  $n$  with a diameter parallel to  $z$ -axis (Fig. 17). The circles  $m, n$  intersect in antipodal points  $U$  and  $W$ , which correspond to fibers  $u$  and  $v$ ,

respectively. These fibers were depicted in Figs. 11 (a) and (b). Therefore, the tori  $\mu$  and  $\nu$  have two common fibers, such that one of its conjugated images is always a segment, and the second image is a great circle. Considering the above-mentioned property of the fiber through the center of stereographic projection ( $u$  in Fig. 17), the stereographic images  $\mu_S$  and  $\nu_S$  of the tori have a common line  $u_S$ .

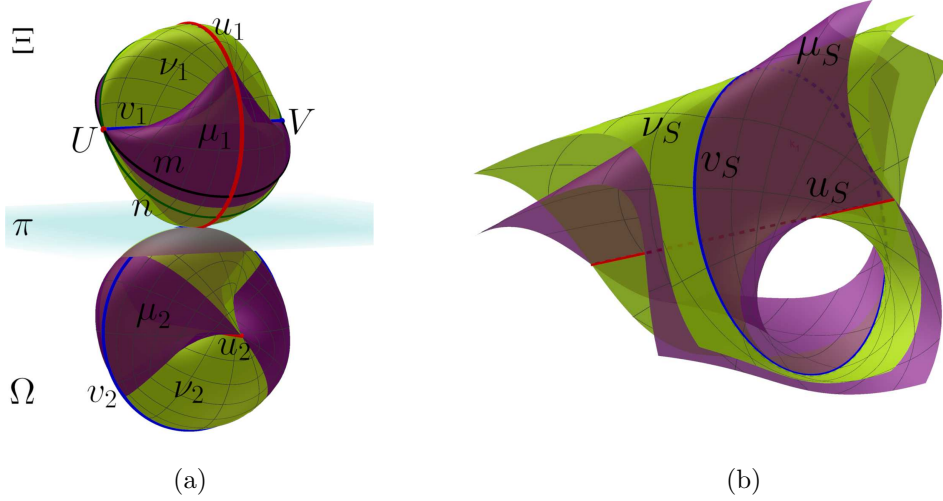


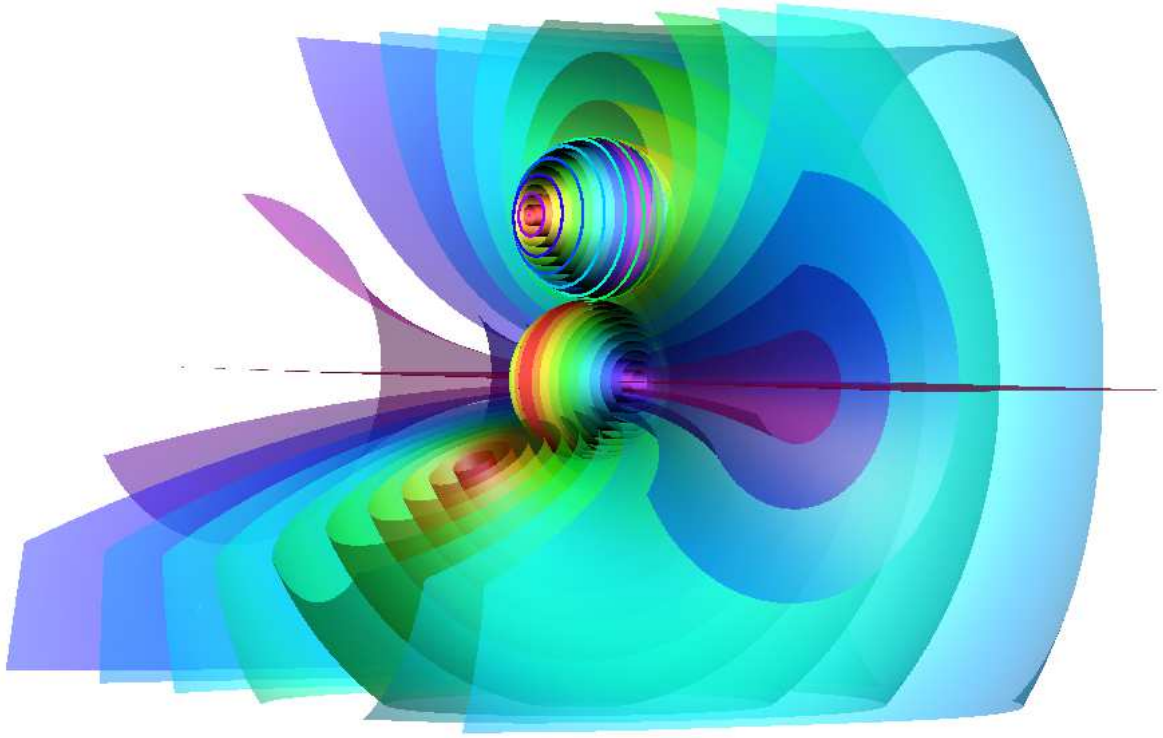
Fig. 17: (a) Conjugated images of the tori  $\mu$  and  $\nu$  corresponding to the circles  $m$  and  $n$ , respectively. The circles  $m, n$  pass through the points  $U, V$  on the diameter of  $\mathcal{B}^2$  parallel to  $z$ -axis. The fibers  $u$  and  $v$  above points  $U$  and  $V$ , respectively, lie on both tori. (b) Stereographic images  $\mu_S$  and  $\nu_S$  of the tori. The stereographic images  $u_S$  and  $v_S$  of the fibers  $u$  and  $v$  are the intersecting line and circle of  $\mu_S$  and  $\nu_S$ .

In the interactive model <https://www.geogebra.org/m/k94dvfpx> (or Supp. File 7), the user can manipulate the circles  $m, n$  with the parameter  $\varphi$  in equation (28). The projections of tori  $\mu$  and  $\nu$  change dependently on  $m, n$ . The visibility of the objects on  $\mathcal{B}^2$ , conjugated images in the double orthogonal projection, or the stereographic image can be turned off.

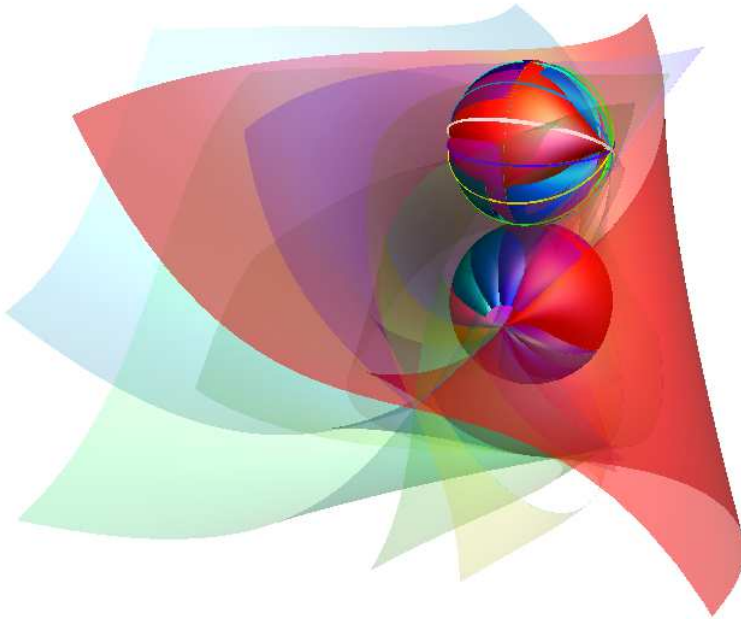
### 5.3 Nested Hopf tori corresponding to families of circles on $\mathcal{B}^2$

Let us summarize the toroidal structure of a 3-sphere in the following visualizations. For each circle  $k$  parallel to  $(x, y)$ -plane on the 2-sphere  $\mathcal{B}^2$ , we obtain a torus  $\kappa$ . In Fig. 18a is a model (see Suppl. File 8 for a video animation) of nested tori  $\kappa$  on  $\mathcal{T}^3$  corresponding to circles  $k$  on  $\mathcal{B}^2$ . This family of disjoint tori contains only one fiber through the center of the stereographic projection, and hence the tori appear in the stereographic projection as nested tori of revolution including one line — their axis.

In the second case (Fig. 18b, Suppl. File 9), the family of circles  $m$  on  $\mathcal{B}^2$  with a diameter parallel to the  $z$ -axis forms nested tori  $\mu$  on  $\mathcal{T}^3$ . Each of these tori contains two common fibers in the special positions as in Fig. 17. The stereographic image of one of the fibers is a line, which is the common line for all the stereographic images of the tori.



(a)



(b)

Fig. 18: A family of circles on  $\mathcal{B}^2$  parallel to  $(x, y)$  (a) and with a diameter parallel to  $z$  (b), the corresponding nested tori on  $\mathcal{T}^3$ , and their stereographic projection to  $\Omega(x, z, w)$ . Colors (shades) refer to mutually related objects, in (b) the images of the torus highlighted in red corresponds to the white great circle on  $\mathcal{B}^2$ . The visualizations are based on the parametrization in equation (31).

These families of tori cover the 3-sphere  $\mathcal{T}^3$  reparametrized with variables  $\beta'$ ,  $\varphi'$ , and  $\psi'$  as:

$$\mathcal{T}^3(\beta', \varphi', \psi') = \begin{pmatrix} \cos \frac{\psi'}{2} \cos(\varphi' + \beta') \\ \cos \frac{\psi'}{2} \sin(\varphi' + \beta') \\ \sin \frac{\psi'}{2} \cos(\beta') \\ \sin \frac{\psi'}{2} \sin(\beta') \end{pmatrix}, \quad (24)$$

$$\beta', \varphi' \in \langle 0, 2\pi \rangle, \psi' \in \langle 0, \pi \rangle.$$

## 5.4 Further issues

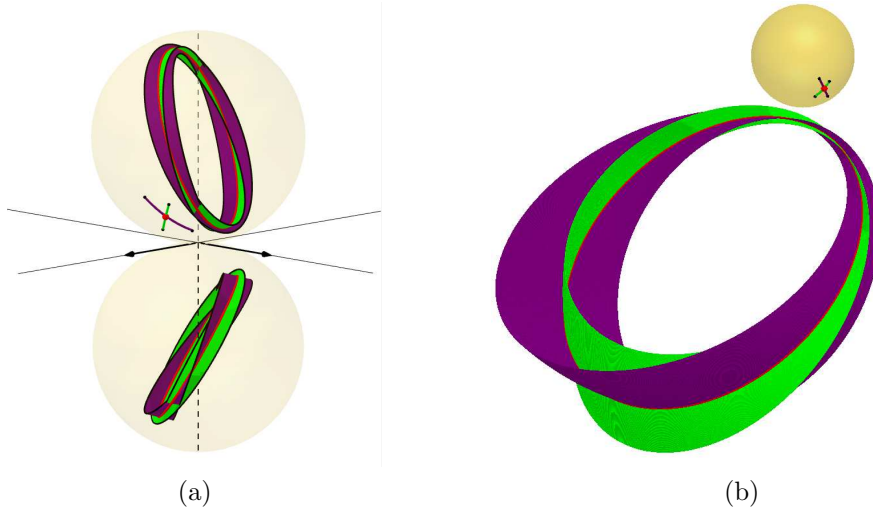


Fig. 19: The intersection point of two curves on a 2-sphere  $\mathcal{B}^2$ . The corresponding fibers in the Hopf fibration form two cyclic surfaces on the 3-sphere  $\mathcal{T}^3$  intersecting in one circle. The situation is visualized in the double orthogonal projection (a) and stereographic projection (b).

Considering the above-mentioned method of visualization and construction of the Hopf fibration, we can study the related properties of geometric surfaces and design shapes formed by disjoint circles. If we consider a point moving along an arbitrary curve on the 2-sphere  $\mathcal{B}^2$ , the motion of the corresponding Hopf fiber creates a cyclic surface consisting of disjoint circles of variable radius on the 3-sphere  $\mathcal{T}^3$  embedded in  $\mathbb{R}^4$ . Consequently, two curves intersecting in one point on a 2-sphere create two cyclic surfaces with only one common circle (the Hopf fiber of the point of intersection) (Fig. 19a). Stereographic projection preserves circles (up to a circle through the center of projection) and so the stereographic images are cyclic surfaces intersecting in a circle in  $\mathbb{R}^3$ , too (Fig. 19b).

At last, we can construct orthogonal and stereographic images of shapes consisting of cyclic surfaces or their parts connected with common circles. The case in Fig. 20 shows a union of three circular arcs (the vertices are tangent points of the corresponding circles)

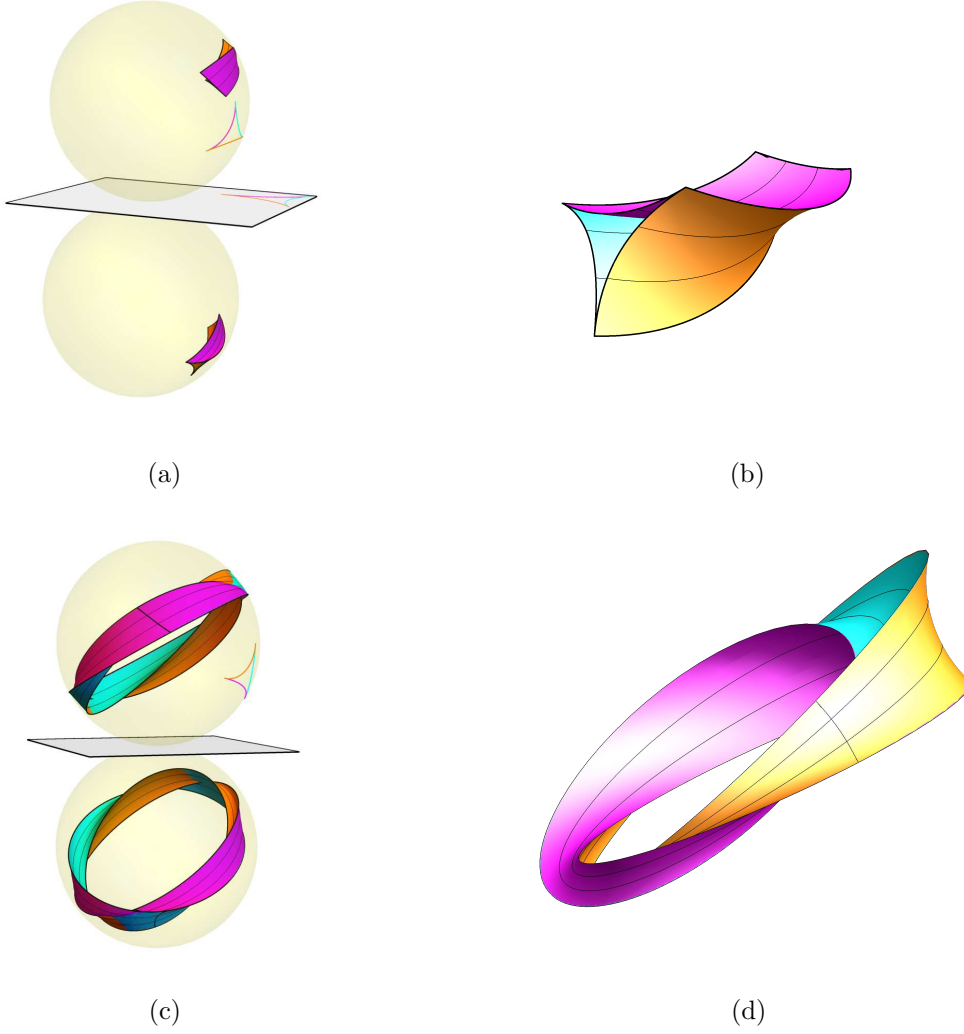


Fig. 20: A planar shape created by three circular arcs in the  $(x, z)$  plane is stereographically projected into the 2-sphere  $\mathcal{B}^2 \in \mathbb{R}^3$ . The corresponding fibers in the Hopf fibration into  $\mathcal{T}^3 \in \mathbb{R}^4$  form three connected parts of cyclic surfaces, each two connected by a common circle. A part of the shape is depicted in the double orthogonal projection (a) and stereographic projection (b). The whole shape is visualized in the double orthogonal projection (c) and stereographic projection (d).

stereographically projected from  $(x, z)$ -plane to a 2-sphere  $\mathcal{B}^2$ . Then, we apply the inverse Hopf projection and construct conjugated images of the corresponding surfaces in  $\mathcal{T}^3$  in the double orthogonal projection. After the stereographic projection from  $\mathcal{T}^3$  to the 3-space  $\Omega(x, z, w)$  we obtain a three-dimensional model of the shape as the union of parts of cyclic surfaces. The common points of each pair of circular arcs become the common circles of each pair of parts of the cyclic surfaces.

## 6 Conclusion

With the use of elementary constructive tools in the double orthogonal projection of the 4-space onto two mutually perpendicular 3-spaces rotated into one 3-dimensional modeling space, we have described a synthetic step-by-step construction of a Hopf fiber on a 3-sphere embedded in the 4-space that corresponds to a point on a 2-sphere. The virtual modeling space is accessible in supplementary interactive models created in the interactive 3D geometric software *GeoGebra 5*, in which the reader can intuitively manipulate fundamental objects and grasp the perception of the fourth dimension through two interlinked 3-dimensional models. The choice of the method of visualization plays a significant role in several aspects. First, two conjugated three-dimensional images of a four-dimensional object carry all the necessary information to determine this object uniquely. For example, if we had only one image of parallel sections of a 3-sphere in Fig. 7b, we would miss important details for reconstruction. Interpretation of two three-dimensional images as one object indeed asks for some training and experience. However, in the case of projection into a plane, we would need at least three images for a visual representation. Another advantage of the double orthogonal projection is that synthetic constructions generalize constructions in Monge's projection. Thus, for example, the localization of a point on a 3-sphere or constructions of stereographic images are elementary. Furthermore, with the use of this technique, we have visualized a torus formed by the Hopf fibers corresponding to a circle on the 2-sphere and demonstrated it in two different positions of the circles on the 2-sphere. The Hopf fibration is usually visualized in the stereographic projection based on an analytic representation. Since the intuition in the four-dimensional visualization, including the double orthogonal projection, is often misleading, stereographic images, in this case, support our reasoning. Therefore, the tori were projected to synthetically constructed stereographic images into the modeling 3-space, revealing the true nature of the Hopf fibration. The final visualizations show how the points of the 2-sphere cover the 3-sphere by their corresponding fibers on the nested tori, and the whole modeling 3-space when stereographically projected. This way, we have built a mathematical visualization of the Hopf fibration, in which we have presented a constructive connection between the base space — 2-sphere, fibers covering the total space — 3-sphere, and the stereographic images, and we can study and explain its properties not dependent on analytic descriptions. However, for verification and implementation, the objects are supported with their parametric representations used in the classical analytic approach.

We have shown a short application of the Hopf fibration for constructing shapes on the 3-sphere and in stereographic projection in the 3-space. The provided method naturally implies the future work in visualizing different curves on a 2-sphere and their corresponding surfaces generated by their Hopf fibers on a 3-sphere in the 4-space and

their corresponding stereographic images in the modeling 3-space. The double orthogonal projection method is also convenient to visualize and analyze the properties of further 3-manifolds embedded in the 4-space.

## 7 Acknowledgment

I wish to thank Lada Peksová (Charles University) for her help with the topological aspects and Filip Beran (Charles University) for revision and valuable suggestions.

## References

- Alvarez, A., Ghys, E., and Leys, J. (2008). *Dimensions Chapter 7 and 8*. Accessed 20 November 2019, (online) <http://www.dimensions-math.org/>.
- Banchoff, T. (1990). *Beyond the third dimension : geometry, computer graphics, and higher dimensions*. Scientific American Library ;W. H. Freeman and Company, New York.
- Banchoff, T. F. (1988). Geometry of Hopf Mapping and Pinkall’s Tori of Given Conformal Type. *Computers in Algebra*, pages 57–62.
- Black, D. V. I. (2010). *Computational Techniques to Enable Visualizing Shapes of Objects of Extra Spatial Dimensions*. PhD thesis, University of California, Irvine.
- Canlubo, C. R. (2017). The Heegaard splitting of  $S^3$  and the Hopf fibration. *Matimyas Matematika*, 40(1-2):13–18.
- Chinyere, I. (2012). *Computer simulation of the modular fibration*. PhD thesis, Stellenbosch University.
- Chu, A., Fu, C. W., Hanson, A. J., and Heng, P. A. (2009). GL4D: A GPU-based architecture for interactive 4D visualization. *IEEE Transactions on Visualization and Computer Graphics*, 15(6):1587–1594.
- Hanson, A. J. (2006). *Visualizing Quaternions: Series in interactive 3D technology*. Morgan Kaufman.
- Hanson, A. J., Ishkov, K. I., and Ma, J. H. (1999). Meshview: Visualizing the Fourth Dimension. Technical report.
- Hatcher, A. (2002). *Algebraic Topology*. Cambridge University Press.
- Heng, P. A. (1992). *Interactive visualization tools for topological exploration*. PhD thesis, Indiana University.

- Hopf, H. (1931). Über die Abbildungen der dreidimensionalen Sphäre auf die Kugelfläche. *Mathematische Annalen*, 104(1):637–665.
- Hopf, H. (1935). Über die Abbildungen von Sphären auf Sphäre niedrigerer Dimension. *Fundamenta Mathematicae*, 25(1):427–440.
- Johnson, N. (2011). *Hopf Fibration Video*. Accessed 20 November 2019, (online) <https://nilesjohnson.net/hopf.html>.
- Koçak, H. and Laidlaw, D. (1987). Computer graphics and the geometry of  $S^3$ . *The Mathematical Intelligencer*, 9(1):8–10.
- Kreminski, R. (1997). *Visualizing the Hopf Fibration*. Accessed 20 November 2019, (online) <https://library.wolfram.com/infocenter/Articles/2944/>, Wolfram Library Archive.
- Lyons, D. W. (2003). An Elementary Introduction to the Hopf Fibration. *Mathematics Magazine*, 76(2):87.
- O’Sullivan, B. (2015). *The Hopf-Fibration and Hidden Variables in Quantum and Classical Mechanics*. Accessed 16 October 2020, (online) <http://arxiv.org/abs/1601.02569>.
- Ozols, M. (2007). *Geometry of a qubit*. Accessed 6 April 2020, (online) [http://home.lu.lv/~sd20008/papers/essays/Geometry \[paper\].pdf](http://home.lu.lv/~sd20008/papers/essays/Geometry[paper].pdf).
- Shoemake, K. (1994). Fiber Bundle Twist Reduction. In Heckbert, P., editor, *Graphics Gems*, pages 230–236. Elsevier.
- Thakur, S. and Hanson, A. J. (2007). A Framework for Exploring High-Dimensional Geometry. In Bebis, G., Boyle, R., Parvin, B., Koracin, D., Paragios, N., Tanveer, S.-M., Tao, J., Liu, Z., Coquillart, S., Cruz-Neira, C., Müller, T., and Malzbender, T., editors, *Advances in Visual Computing, ISVC, Lecture Notes in Computer Science*, pages 804–815. Springer, Berlin, Heidelberg.
- Treisman, Z. (2009). *A young person’s guide to the Hopf fibration*. Accessed 27 November 2019, (online) <http://arxiv.org/abs/0908.1205>.
- Tsai, L.-Y. (2006). *Hopf Fibration, Manifold I, Manifold II*. Accessed 16 October 2020, <http://lunyitsai.com/paintings/>.
- Yershova, A., Jain, S., LaValle, S. M., and Mitchell, J. C. (2010). Generating Uniform Incremental Grids on  $SO(3)$  Using the Hopf Fibration. *The International Journal of Robotics Research*, 29(7):801–812.



- Zamboj, M. (2018a). Double Orthogonal Projection of Four-Dimensional Objects onto Two Perpendicular Three-Dimensional Spaces. *Nexus Network Journal*, 20(1):267–281.
- Zamboj, M. (2018b). Sections and Shadows of Four-Dimensional Objects. *Nexus Network Journal*, 20(2):475–487.
- Zamboj, M. (2019a). 1-2-3-Sphere in the 4-Space. In *Proceedings of Slovak-Czech Conference on Geometry and Graphics 2019*, pages 217–222, Plzeň. Vydavatelský servis.
- Zamboj, M. (2019b). Quadric Sections of Four-Dimensional Cones. In *Advances in Intelligent Systems and Computing*, volume 809, pages 500–513. Springer, Cham.
- Zamboj, M. (2019c). *Visualization of the Hopf fibration*,. Accessed 16 October 2020, <https://www.geogebra.org/m/x5pev89m>.
- Zhang, H. and Hanson, A. J. (2007). Shadow-driven 4D haptic visualization. *IEEE Transactions on Visualization and Computer Graphics*, 13(6):1688–1695.
- Zhou, J. (1991). *Visualization of Four Dimensional Space and Its Applications*. PhD thesis, Purdue University.

## A Parametrization relevant to the figures

We give parametrization in  $\mathbb{R}^4$  with  $(x, y, z, w)$ -coordinates in the following lines. For the implementation to visualizations in the double orthogonal projection in the modeling space with  $(x, y, z)$ -coordinates, we decompose the images such that a  $\Xi$ -image has  $(x, y, z)$ -coordinates, and an  $\Omega$ -image has  $(x, -w, z)$ -coordinates.

### Figs. 10 and 14

A point  $Q$  on the 2-sphere  $\mathcal{B}^2$  (cf. Equation 13)

$$Q = \begin{pmatrix} \sin \psi \cos \varphi \\ \sin \psi \sin \varphi + 1 \\ \cos \psi \end{pmatrix}, \quad (25)$$

$$\psi \in \langle 0, \pi \rangle, \varphi \in \langle 0, 2\pi \rangle.$$

Further on  $\psi$  and  $\varphi$  are fixed, and  $\gamma = \frac{\psi}{2}, \varphi = \alpha - \beta$ , for  $\beta \in \langle 0, 2\pi \rangle$ .

A point  $P$  on the 3-sphere  $\mathcal{T}^3$  (cf. Equation 14)

$$P = \begin{pmatrix} \cos \frac{\psi}{2} \cos(\varphi + \beta) \\ \cos \frac{\psi}{2} \sin(\varphi + \beta) + 1 \\ \sin \frac{\psi}{2} \cos \beta \\ \sin \frac{\psi}{2} \sin \beta + 1 \end{pmatrix}, \quad (26)$$

and also the parametrization of the circle  $c(\beta)$  for the variable  $\beta$ .

The point  $P_S$  in  $\Omega(x, z, w)$  — the stereographic image of the point  $P$  from the center  $N = [0, 2, 0, 1]$

$$P_S = \begin{pmatrix} \frac{2 \cos \frac{\psi}{2} \cos(\varphi + \beta)}{1 - \cos \frac{\psi}{2} \sin(\varphi + \beta)} \\ \frac{2 \sin \frac{\psi}{2} \cos \beta}{1 - \cos \frac{\psi}{2} \sin(\varphi + \beta)} \\ \frac{2 \sin \frac{\psi}{2} \sin \beta}{1 - \cos \frac{\psi}{2} \sin(\varphi + \beta)} + 1 \end{pmatrix}, \quad (27)$$

and also the parametrization of the circle  $c_S(\beta)$  for the variable  $\beta$ .

### Figs. 15 and 16

A circle  $k$  on  $\mathcal{B}^2$  for a fixed  $\psi$  (cf. Equation 20)

$$k(\varphi') = \begin{pmatrix} \sin \psi \cos \varphi' \\ \sin \psi \sin \varphi' \\ \cos \psi + 1 \end{pmatrix}, \quad \varphi' \in \langle 0, 2\pi \rangle. \quad (28)$$

The torus  $\kappa$  corresponding to the circle  $k$  (cf. Equation 21)

$$\kappa(\beta', \varphi') = \begin{pmatrix} \cos \frac{\psi}{2} \cos(\varphi' + \beta') \\ \cos \frac{\psi}{2} \sin(\varphi' + \beta') + 1 \\ \sin \frac{\psi}{2} \cos(\beta') \\ \sin \frac{\psi}{2} \sin(\beta') + 1 \end{pmatrix}, \beta', \varphi' \in \langle 0, 2\pi \rangle. \quad (29)$$

The stereographic image of the torus  $\kappa$  in  $\Omega(x, z, w)$  (cf. Equation 24)

$$\kappa(\beta', \varphi') = \begin{pmatrix} \frac{2 \cos \frac{\psi}{2} \cos(\varphi' + \beta')}{1 - \cos \frac{\psi}{2} \sin(\varphi' + \beta')} \\ \frac{2 \sin \frac{\psi}{2} \cos(\beta')}{1 - \cos \frac{\psi}{2} \sin(\varphi' + \beta')} \\ \frac{2 \sin \frac{\psi}{2} \sin(\beta')}{1 - \cos \frac{\psi}{2} \sin(\varphi' + \beta')} + 1 \end{pmatrix}, \beta', \varphi' \in \langle 0, 2\pi \rangle. \quad (30)$$

Analogously, a circle  $m$ , torus  $\mu$  with their stereographic images differ to  $k$  and  $\kappa$  only by fixing  $\varphi$  and the variable  $\psi'$ .

### Fig. 18

The stereographic images of the nested tori in  $\Omega(x, z, w)$  have the following parametric representation (cf. Equation 24):

$$\mathcal{T}^3(\beta', \varphi', \psi') = \begin{pmatrix} \frac{2 \cos \frac{\psi'}{2} \cos(\varphi' + \beta')}{1 - \cos \frac{\psi'}{2} \sin(\varphi' + \beta')} \\ \frac{2 \sin \frac{\psi'}{2} \cos(\beta')}{1 - \cos \frac{\psi'}{2} \sin(\varphi' + \beta')} \\ \frac{2 \sin \frac{\psi'}{2} \sin(\beta')}{1 - \cos \frac{\psi'}{2} \sin(\varphi' + \beta')} + 1 \end{pmatrix}. \quad (31)$$

The stereographic image in Fig. 18a is for the sake of clarity bounded to  $\beta' \in \langle \frac{\pi}{6}, \frac{3\pi}{2} \rangle$ , and the leading variable is chosen  $\psi' = k \frac{\pi}{12}$  for  $k \in \{0, 1, \dots, 12\}$ . In Fig. 18b the  $\Xi$  and  $\Omega$ -images  $\mu_1$  and  $\mu_2$  of the tori  $\mu$  are, apart of the one highlighted in red, bounded to  $\beta' \in \langle \frac{\pi}{3}, \frac{5\pi}{3} \rangle, \psi' \in \langle \frac{\pi}{6}, 2\pi \rangle$ , the stereographic images to  $\beta' \in \langle \frac{\pi}{6}, 11\frac{\pi}{6} \rangle$ , and the leading variable is  $\varphi' = k \frac{\pi}{6}$  for  $k \in \{0, 1, \dots, 6\}$ .